HHS Public Access

Author manuscript

*Nat Cell Biol*. Author manuscript; available in PMC 2020 August 03.

Published in final edited form as:

*Nat Cell Biol*. 2020 February ; 22(2): 246–256. doi:10.1038/s41556-020-0463-6.

# LATS suppresses mTORC1 activity to directly coordinate Hippo and mTORC1 pathways in growth control

**Wenjian Gan**[1,2,13,*], **Xiaoming Dai**[1,13], **Xiangpeng Dai**[1], **Jun Xie**[3], **Shasha Yin**[2], **Junjie Zhu**[4], **Chen Wang**[4], **Yuchen Liu**[5], **Jianping Guo**[1], **Min Wang**[1,11], **Jing Liu**[1], **Jia Hu**[1,12], **Ryan J. Quinton**[9,10], **Neil J. Ganem**[9,10], **Pengda Liu**[6], **John M. Asara**[7], **Pier Paolo Pandolfi**[8], **Yingzi Yang**[5], **Zhigang He**[4], **Guangping Gao**[3], **Wenyi Wei**[1,*]

[1]Department of Pathology, Beth Israel Deaconess Medical Center, Harvard Medical School, Boston, MA 02215, USA

[2]Department of Biochemistry and Molecular Biology, Medical University of South Carolina, Charleston, SC 29425, USA

[3]Li Weibo Institute for Rare Diseases Research and Horae Gene Therapy Center and Vector Core, University of Massachusetts Medical School, Worcester, MA 01605, USA

[4]F.M. Kirby Neurobiology Center, Boston Children's Hospital and Department of Neurology, Harvard Medical School, 300 Longwood Avenue, Boston, MA 02115, USA

[5]Department of Developmental Biology, Harvard Stem Cell Institute, Harvard School of Dental Medicine, Boston, MA 02215, USA

[6]Department of Biochemistry and Biophysics, Lineberger Comprehensive Cancer Center, The University of North Carolina at Chapel Hill, NC 27599, USA

[7]Division of Signal Transduction, Beth Israel Deaconess Medical Center and Department of Medicine, Harvard Medical School, Boston, MA 02215, USA

[8]Cancer Research Institute, Beth Israel Deaconess Cancer Center, Department of Medicine and Pathology, Beth Israel Deaconess Medical Center, Harvard Medical School, Boston, MA 02215, USA

[9]The Laboratory of Cancer Cell Biology, Department of Pharmacology and Experimental Therapeutics, Boston University School of Medicine, Boston, MA 02118, USA

[10]Division of Hematology and Oncology, Department of Medicine, Boston University School of Medicine, Boston, MA 02118, USA



[*]Correspondence: ganw@musc.edu, wwei2@bidmc.harvard.edu.

Author contributions

W.G. and W.W. designed the experiments. W.G. and X.M.D. performed the experiments with assistance from X.P.D., S.Y., J.G., M.W., J.L. J.H., R.J.Q., N. J. G. and P.L. J.M.A. performed the LC-MS/MS metabolomic profiling and mass spectrometry analysis of Raptor S606 phosphorylation. J.X., J.Z., C.W., Y.L., Y.Y, Z.H. and G.G helped to design and perform the experiments on AAV-mediated depletion of *Nf2* and *Lats1/2*. W.W. and P.P.P supervised the study. W.G. and W.W. wrote the manuscript. All authors commented on the manuscript.

Competing interests

The authors declare no competing interests.

[11]Departments of Biliary-Pancreatic Surgery, Affiliated Tongji Hospital, Tongji Medical College, Huazhong University of Science and Technology, Wuhan, Hubei 430030, China

[12]Departments of Urology, Affiliated Tongji Hospital, Tongji Medical College, Huazhong University of Science and Technology, Wuhan, Hubei 430030, China

[13]These authors contributed equally: Wenjian Gan, Xiaoming Dai

## Abstract

The Hippo and mTORC1 pathways are the two predominant growth-control pathways that dictate proper organ development. We therefore explored a possible crosstalk between these two functional relevant pathways to coordinate their growth-control functions. We found that the LATS1/2 kinases, the core component of the Hippo pathway, phosphorylate Ser606 of Raptor, an essential component of mTORC1, to attenuate mTORC1 activation through impairing Raptor interaction with Rheb. The phosphomimetic Raptor-S606D knock-in mutant leads to a reduction in cell size and cell proliferation. Compared to *Raptor*$^{+/+}$ mice, *Raptor*$^{D/D}$ knock-in mice exhibit smaller liver and heart, and a significant inhibition of *Nf2* or *Lats1/2* loss-induced elevation of mTORC1 signaling and liver size. Thus, our study reveals a direct link between the Hippo and mTORC1 pathways to fine-tune organ growth.

Coordination of cell number and cell size is crucial for proper organ growth and body development[1, 2]. To this end, the Hippo and the mammalian target of rapamycin (mTOR) signaling pathways are highly conserved from Drosophila to human and have been characterized as the two predominant pathways controlling tissue/organ size by governing cell number and cell size, respectively[3-6]. Deregulation of either the Hippo pathway or the mTOR pathway leads to tissue overgrowth[5, 7, 8].

The Hippo pathway controls tissue/organ development by regulating a variety of fundamental biological processes, including cell proliferation/division, apoptosis and differentiation[9]. In mammals, the core of the Hippo pathway is composed of a kinase cascade including MST1/2 (homologs of Hpo), MAP4Ks, TAO kinases and LATS1/2 (Wts ortholog), the key regulator NF2 (Merlin), and the well-characterized downstream targets Yes-associated protein (YAP) (Yki orthologs) and TAZ. Mechanistically, MSTs/MAP4Ks/TAO/NF2-mediated activation of LATS1/2 directly phosphorylates YAP/TAZ, leading to their cytoplasmic retention[10]. The Hippo pathway is regulated by several upstream signals including mechanical signals such as cell-cell contact, soluble factors such as LPA/S1P via G protein-coupled receptors (GPCRs), cell polarity and cell adhesion[11].

The mTOR signaling pathway plays a central role in controlling cell growth by sensing four major signals: energy, nutrients, growth factors and stress. mTOR forms two functionally distinct complexes, termed mTORC1 and mTORC2. They share two common subunits, mTOR and mLST8 (also called GβL). Raptor is the specific subunit of mTORC1, while Rictor and Sin1 define mTORC2[12]. mTORC1 serves as a master regulator of protein, lipid and nucleotide synthesis, metabolism and autophagy[13]. It executes biological function by phosphorylating downstream substrates including eukaryotic initiation factor 4E-binding protein 1 (4E-BP1), ribosomal protein S6 kinase 1 (S6K1), Unc-51 Like autophagy

activating kinase 1 (ULK1) and many others[12]. Extensive studies in the past decade significantly expand the understanding of amino acid sensing by mTORC1. Upon amino acid stimulation, mTORC1 is recruited to lysosome by Rag GTPases and subsequently interacts with growth factor-induced Rheb GTPase for fully activation[14].

Given functional relevance of the Hippo and mTORC1 pathways in growth control, emerging evidence suggests that the Hippo and mTOR pathways influence each other[6]. However, the direct molecular mechanism(s) underlying how these two pathways coordinately regulate cell number and cell size to control organ/tissue size remains largely unknown. Here we report that the LATS1/2 kinases, a core component of the Hippo pathway, directly phosphorylates Ser606 of Raptor, an essential component of mTORC1, to attenuate mTORC1 kinase activation in part through impairing Raptor interaction with its activator, Rheb. Therefore, our study reveals a direct crosstalk between the Hippo and mTORC1 signaling pathways, which coordinates these two major growth controlling pathways to timely govern cell size and number to control organ size.

## Results

### LATS1/2 are required for Hippo pathway mediated-suppression of mTORC1 signaling

To investigate a potential interplay between the Hippo and mTOR pathways, we first examined whether mTOR kinase activity was affected by increasing cell density that is known to activate the Hippo pathway[15]. In multiple cell lines, we observed that high cell density decreased the phosphorylation of S6K1 (pS6K1), 4E-BP1 (p4E-BP1) and ULK1, coupled with elevated phosphorylation of YAP (Fig. 1a; Extended Data Fig. 1a-e). Notably, the observed reduction of mTORC1 signaling by increased cell density was unlikely due to deficiency of nutrients in our experimental conditions (Extended Data Fig. 1f). Consistently, treatment of 293A cells with two Hippo pathway activators-Latrunculin B (LatB) and Forskolin (FSK)[16] also resulted in a decreased pS6K1 and p4E-BP1 (Extended Data Fig. 1g). A previous study showed that the Hippo pathway suppresses mTOR activity through YAP/miR-29-mediated downregulation of PTEN, a negative regulator of both mTORC1 and mTORC2[17]. However, we found that in contrast to the dramatic decrease in mTORC1 activity, mTORC2 activity as measured by phosphorylation of Akt at Ser473 (Akt-pS473), was only moderately decreased in HeLa cells under high cell density condition, but not in other cells we examined (Extended Data Fig. 1a-d). Moreover, *PTEN* knockout failed to restore pS6K1 and p4E-BP1 in HEK293 cells at high cell density, or when treated with LatB or FSK (Extended Data Fig. 1h-j). We further found that depletion of *YAP/TAZ* has minor effects on mTORC1 activity in HEK293 cells (Extended Data Fig. 1k-m). These results together indicate that in our experimental setting, the Hippo pathway primarily suppresses mTORC1, but not mTORC2 activity, independent of YAP/TAZ and PTEN through a yet unidentified mechanism. Thus, in the remainder of this study, we focused on understanding mechanistically how the Hippo pathway inhibits the mTORC1 activity and its physiological functions.

We observed that high cell density or LatB/FSK-mediated inhibition of mTORC1 signaling was largely attenuated in cells depleted the Hippo core components LATS1/2, but not its upstream regulators MST1/2, MAP4K4/6/7 or SAV1 (Fig. 1b-d; Extended Data Fig. 2a-d).

Notably, knockout of *MST1/2MAP4K1/2/3/4/6/7* (8 KO) resulted in a more robust inactivation of LATS1/2 and restored mTORC1 signaling under high cell density, LatB or FSK treatment conditions (Fig. 1d; Extended Data Fig. 2a,b). Moreover, depletion of *NF2*, another key Hippo pathway component that activates LATS1/2[18-20], also largely rescued cell confluence- and LatB-mediated suppression of mTORC1 (Fig. 1e; Extended Data Fig. 2e). These results support the notion that LATS kinase activity, tightly governed by Hippo pathway, is required for Hippo-mediated suppression of mTORC1. Moreover, overexpression of LATS1 blocked mTORC1 activation induced by LPA or S1P[16] (Extended Data Fig. 2f). Consistently, re-introducing wild type, but not the kinase-dead form of LATS1 (S909A/T1079A, AA)[21], could largely restore pS6K1 regulation by cell density in *LATS1/2* dKO cells (Extended Data Fig. 2g). Furthermore, immunopurified mTORC1 from *LATS1/2* dKO cells exhibited relatively elevated kinase activity towards phosphorylating S6K1 and 4E-BP1 *in vitro* (Fig. 1f; Extended Data Fig. 2h). These results suggest that the LATS1/2 kinases, but not its upstream regulators, are likely the major component through which the Hippo pathway suppresses mTORC1 signaling.

## LATS1/2 interact with and phosphorylate Raptor at Ser606

Consistently, we found that LATS1 specifically bound Raptor, but not mTOR nor GβL (Fig. 2a,b). Compared with Raptor, LATS1 displayed a much weaker interaction with either Rictor or Sin1 (Fig. 2a). We further identified that LATS1 bound the central region containing HEAT repeats (MH), but not the N-terminus (N) nor WD40 repeats domain (WD40) of Raptor (Extended Data Fig. 3a,b). Upon a closer examination of the Raptor-MH domain protein sequence, we identified an evolutionally conserved putative LATS phosphorylation consensus motif[22] (Fig. 2c). High-resolution liquid chromatography-tandem mass spectrometry (LC-MS/MS) analyses revealed that Ser606 (S606) is phosphorylated in cells (Extended Data Fig. 3c). Mutating S606 to alanine (S606A) largely diminished LATS1-mediated phosphorylation of Raptor *in vitro* (Fig. 2d). We further developed and validated a phospho-specific antibody against Raptor-pS606 (Extended Data Fig. 3d,e), through which we found that the S606A mutation markedly blocked phosphorylation of S606 *in vitro* and in cells (Fig. 2d,e; Extended Data Fig. 3f). Moreover, Raptor-pS606 was largely abolished in *LATS1/2* dKO cells (Fig. 2f,g; Extended Data Fig. 3g,h). Furthermore, LATS1, but not other kinases we examined including JNK1, JNK2, CaMKK1, CaMK2β, CaMK4, NEK6 and NEK7, specifically interacted with Raptor and phosphorylated S606 in cells (Fig. 2h; Extended Data Fig. 3i,j), confirming LATS being the major kinase responsible for phosphorylating Raptor-S606. Notably, the mTORC1 complex immunopurified from HEK293 cells ectopically expressing the phosphomimetic mutant, Raptor-S606D (termed S606D thereafter), displayed a reduction in mTOR kinase activity towards phosphorylating 4E-BP1 *in vitro*, compared with the mTORC1 complex containing WT-Raptor (Extended Data Fig. 3k). These results together indicate that Raptor-S606 is the major LATS phosphorylation site, and its phosphorylation may play a critical role in mediating LATS-dependent inhibition of mTORC1 kinase activity.

## LATS1/2-mediated phosphorylation of Raptor-Ser606 attenuates mTORC1 activation

To better understand the biological function of Raptor-S606 phosphorylation by the LATS1/2 kinases, we generated Raptor-S606D or Raptor-S606A knock-in cell lines (termed

S606D$^{knock\text{-}in}$ and S606A$^{knock\text{-}in}$, respectively) using the CRISPR/Cas9 genome-editing technology (Extended Data Fig. 4a-c). Notably, HEK293 and 293E cells harboring the S606D mutation, but not the S606A mutation, displayed a dramatic reduction in mTORC1 signaling (Extended Data Fig. 4d,e). Consistent with escaping Hippo-mediated mTORC1 inhibition, S606A$^{knock\text{-}in}$ cells could largely overcome cell confluence, LatB or FSK-mediated suppression of mTORC1, whereas S606D$^{knoc\text{-}in}$ cells displayed a reduction in mTORC1 kinase activity even in low cell density condition (Fig. 3a; Extended Data Fig. 4f,g). This was coupled with an elevation of Raptor-pS606 in WT, but not S606A$^{knock\text{-}in}$ cells (Fig. 3b; Extended Data Fig. 4f,g). In keeping with these results, we further found that *in vitro* kinase activity derived from immunopurified mTORC1 complex containing the Raptor-S606D mutation was much lower than mTORC1 complex associated with Raptor-WT (Fig. 3c; Extended Data Fig. 4h). In addition, ectopic overexpression of YAP1 or depletion of *YAP/TAZ* had minor effects on mTORC1 activity in both WT and S606D$^{knock\text{-}in}$ cells (Extended Data Fig. 4i,j), further supporting a likely YAP/TAZ-independent mechanism for the Hippo pathway in regulating mTORC1 activation.

Next, we investigated whether Raptor-S606 phosphorylation affects growth factor and amino acid- induced activation of mTORC1. Interestingly, we found that growth factors such as insulin or IGF-1 were incapable of fully activating mTORC1 in serum-starved S606D$^{knock\text{-}in}$ cells as they did in WT and S606A$^{knock\text{-}in}$ cells (Fig. 3d; Extended Data Fig. 5a,b), which mimics partial knockdown of *Rheb* (Extended Data Fig. 5c). Interestingly, the lysosomal localization of mTORC1 was unaffected in S606D$^{knock\text{-}in}$ cells in response to amino acid deprivation and stimulation (Fig. 3e). However, amino acid stimulation failed to fully activate mTORC1 in S606D$^{knock\text{-}in}$ cells largely due to its deficiency in responding to growth factors (Fig. 3f), which is consistent with the notion that both amino acids and growth factors are required for the robust activation of mTORC1[23]. In keeping with a critical role for Rheb in activating mTORC1 upon growth factor stimulation[24], ectopic expression of Rheb-WT or a constitutively active form of Rheb (Q64L), but not the inactive forms of Rheb (S20N and D60I), could induce pS6K1 under serum starvation condition (Extended Data Fig. 5d). Moreover, the S606D mutation attenuated Rheb-Q64L-induced mTORC1 activation (Fig. 3g). Consistently, the LATS1-WT, but not the kinase dead mutant form of LATS1-AA, markedly inhibited Rheb, but not RagB-induced mTORC1 activation under serum starvation or amino acid deprivation/stimulation conditions, respectively (Extended Data Fig. 5e,f), indicating that LATS1 largely inhibits mTORC1 kinase activity by interfering with the function of Rheb on activating mTORC1 in a kinase activity-dependent manner. Notably, depletion of *DEPTOR* elevated mTORC1 activity in WT, but not S606D$^{knock\text{-}in}$ cells (Extended Data Fig. 5g), suggesting that DEPTOR is dispensable for Raptor-pS606-mediated suppression of mTORC1. Moreover, depleting endogenous *TSC2*, the upstream GAP negatively regulating Rheb[25, 26], efficiently elevated pS6K1 in serum-deprived WT and S606A$^{knock\text{-}in}$ cells, but not S606D$^{knock\text{-}in}$ cells (Extended Data Fig. 5h). Furthermore, LatB markedly blocked pS6K1 in *Tsc2*$^{-/-}$ MEFs under serum starvation (Extended Data Fig. 5i). Consistently, we found that recombinant Rheb proteins efficiently induced the kinase activity of the mTORC1 complex immunopurified from cells expressing Raptor-WT, but not the Raptor-S606D mutant, in a GTP loading-dependent manner *in vitro* (Fig. 3h; Extended Data Fig. 5j). These results suggest that LATS-mediated phosphorylation

of S606 diminishes growth factor-induced activation of mTORC1 through Rheb (Extended Data Fig. 5k).

## Phosphorylation of Raptor-Ser606 modulates its interaction with Rheb and DEPTOR

Given the essential role of Raptor and Rheb in determining mTORC1 kinase activity[27-29], we next sought to dissect the molecular mechanism(s) by which S606 phosphorylation of Raptor inhibits mTORC1. To this end, we generated an N-terminal Flag-tagged version of endogenous Raptor by CRISPR in WT, S606D$^{knock\text{-}in}$ and S606A$^{knock\text{-}in}$ cells, respectively. Compared with Raptor-WT and S606A, the S606D mutation did not significantly affect its interaction with endogenous mTOR and GβL in cells (Extended Data Fig. 6a,b), indicating that the S606D mutation likely inhibits mTORC1 kinase activity through modulating Raptor interaction with mTORC1 regulators, but not the integrity of the core mTORC1 complex *per se*. In this regard, previous studies have identified the Rheb and Rag family of small GTPases as the key activators of mTORC1 in response to growth factors and amino acids, respectively[24, 30]. In keeping with the result that S606D suppresses growth factor-induced activation of mTORC1 but not amino acid-induced mTORC1 lysosome localization, we found that S606D dramatically decreased Raptor interaction with Rheb (Fig. 4a; Extended Data Fig. 6c), but not Rag GTPases in cells (Extended Data Fig. 6d). In addition to these two activators, PRAS40 and DEPTOR, two well-characterized endogenous inhibitors of mTORC1, suppress mTORC1 activation in response to growth factors[29, 31]. Interestingly, the S606D mutation enhanced Raptor binding with DEPTOR (Fig. 4b; Extended Data Fig. 6e), but not PRAS40 (Extended Data Fig. 6f). In line with these findings, the interaction between Raptor and Rheb was decreased, whereas Raptor binding to DEPTOR was conversely elevated, by LATS1-WT, but not LATS1-AA (Fig. 4c,d), in a Raptor-S606 phosphorylation-dependent manner (Extended Data Fig. 6g,h). Consistently, high cell density, LatB or FSK decreased Raptor interaction with Rheb, whereas induced the interaction between Raptor and DEPTOR, in Raptor-WT, but not S606A$^{knock\text{-}in}$ cells (Fig. 4e,f; Extended Data Fig. 6i-m).

Consistent with a critical role for Raptor-pS606 in determining Raptor interaction with Rheb and DEPTOR, but not Rags and PRAS40, we found that Rag GTPases and PRAS40 primarily interacted with the N-terminus of Raptor (Extended Data Fig. 7a-c), whereas Rheb largely bound to the MH domain where S606 resides (Fig. 4g), and DEPTOR associated with both MH domain and WD40 domain (Extended Data Fig. 7d,e). Moreover, ectopically expressed Rheb disrupted Raptor interaction with DEPTOR, but not PRAS40, in a dose-dependent manner in cells (Fig. 4h; Extended Data Fig. 7f). To exclude a possible contribution of reduced mTORC1 kinase activity in causing the observed interaction changes between the Raptor-S606 mutants and various mTORC1 regulators, we treated cells with the mTOR inhibitor, Torin1[32], and observed that Torin1 only minimally affected Raptor interaction with DEPTOR, Rheb and RagC in cells (Extended Data Fig. 7g,h). All together, these results suggest that phosphorylation of Raptor-S606 by LATS1/2 disrupts Raptor interaction with Rheb and conversely, enhances its binding with DEPTOR to suppress mTORC1 kinase activity.

## Deficiency in Raptor-S606 phosphorylation alters cell metabolism, growth and proliferation

It is well established that mTORC1 is a central regulator of protein synthesis, metabolism and lipid biogenesis[33]. We next examined how the S606D mutation affects these mTORC1-governed cellular processes. Notably, using a high-throughput liquid chromatography mass spectrometry (LC-MS) metabolomics approach, we found that consistent with a sharp decrease of mTORC1 kinase activity[34], the intermediates of glycolysis and the pentose phosphate pathways were decreased in S606D$^{knock\text{-}in}$ cells compared to WT and S606A$^{knock\text{-}in}$ cells (Fig. 5a), accompanied by significantly decreased mRNA levels of representative genes of the glycolysis and pentose phosphate pathways (Fig. 5b,c). Consistently, as assessed by the extracellular acidification rate (ECAR) with seahorse analysis, compared to WT and S606A$^{knock\text{-}in}$ cells, the maximal glycolytic capacity of S606D$^{knock\text{-}in}$ cells was significantly reduced (Fig. 5d,e). Furthermore, the S606D mutant also appeared to reduce *de novo* lipid biosynthesis in part by suppressing the expression of key enzymes involved in this process (Fig. 5f). Notably, overexpression of LATS1-WT, but not the kinase-dead LATS1-AA, phenocopied the metabolic defects exhibited in S606D$^{knock\text{-}in}$ cells (Fig. 8g-i). These data coherently suggest that phosphorylation of Raptor-S606 by the key Hippo component LATS1/2 kinase, negatively regulates glycolysis and lipid biosynthesis, both of which are characterized physiological downstream readouts of the mTORC1 kinase complex[33, 35].

In keeping with the role of mTORC1 on cell size control, and an observed reduction of mTORC1 activity in S606D$^{knock\text{-}in}$ cells (Fig. 3a), S606D$^{knock\text{-}in}$ cells were relatively smaller than WT and S606A$^{knock\text{-}in}$ cells (Fig. 6a). Moreover, compared to WT cells, S606A$^{knock\text{-}in}$ cells were partially resistant to cell density-induced reduction of cell size (Extended Data Fig. 8a). Furthermore, S606D$^{knock\text{-}in}$ cells displayed a dramatic decrease in cell proliferation (Extended Data Fig. 8b) and colony formation regarding both colony number and colony size (Fig. 6b; Extended Data Fig. 8c). Notably, *LATS1/2* knockout failed to elevate mTORC1 activity and colony formation of S606D$^{knock\text{-}in}$ cells (Fig. 6c,d). On the other hand, overexpression of LATS1-WT, but not LATS1-AA, suppressed mTORC1 signaling and colony formation of WT cells, but not S606A$^{knock\text{-}in}$ cells (Fig. 6e,f). To explore the role of LATS-mediated phosphorylation of Raptor in tumorigenesis, we attempted to generate the S606D$^{knock\text{-}in}$ HeLa or HCT116 cells for *in vivo* xenograft tumor growth assay. Unfortunately, we could not obtain such knock-in cell lines due to technical difficulties. However, several Raptor knockout HCT116 cell lines (*Raptor*$^{KO}$) were generated as evidenced by the absence of Raptor, pS6K1 and p4E-BP1 (Extended Data Fig. 8d). As a result, these *Raptor*$^{KO}$ cells exhibited a significant reduction in colony formation (Extended Data Fig. 8e) and anchorage-independent cell growth (Extended Data Fig. 8f). Importantly, compared with reconstitution of Raptor-WT and Raptor-S606A, reconstitution of Raptor-S606D only partially restored pS6K1 and p4E-BP1 in *Raptor*$^{KO}$ cells (Fig. 6g), as well as colony formation (Fig. 6h) and anchorage-independent cell growth (Fig. 6i). Consistently, compared with *Raptor*$^{KO}$ cells expressing Raptor-WT, *Raptor*$^{KO}$ cells expressing Raptor-S606D mutant displayed retarded tumor growth in a xenograft mouse model (Fig. 6j,k; Extended Data Fig. 8g). These results together suggest that phosphorylation of Raptor-S606 by LATS1/2 impairing mTORC1 signaling in part mediates the inhibitory effect of the Hippo pathway on cell growth and proliferation.

### Hippo pathway controls organ size in part through suppressing mTORC1 signaling via Raptor

To further understand the physiological function of LATS1/2-mediated phosphorylation of Raptor *in vivo*, we generated homozygous phosphomimetic (S606D; $Raptor^{D/D}$) knock-in mice in C57BL/6J background using CRISPR/Cas9 technology (Extended Data Fig. 9a-c). $Raptor^{D/D}$ mice were born at the expected Mendelian ratio (Extended Data Fig. 9d). Notably, both male and female $Raptor^{D/D}$ mice exhibited about 5–10% lower body weight than WT littermates up to 8 weeks of age (Extended Data Fig. 9e-g). Consistent with the observation that S606D mutation suppresses the expression of key enzymes involved de novo lipid biosynthesis (Fig. 5f), $Raptor^{D/D}$ mice were resistant to high-fat diet (HFD)-induced obesity and accumulation of hepatic lipid droplets, compared to WT littermates (Extended Data Fig. 9h-k). Moreover, $Raptor^{D/D}$ mice displayed markedly decreased mTORC1 signaling in liver, heart and kidney, but not in spleen and brain for reasons not fully understood (Fig 7a,b; Extended Data Fig. 9l). Notably, $Raptor^{D/D}$ mice exhibited smaller liver, heart and kidney, compared with WT littermates (Fig. 7c), which is in part due to the decreased mTORC1 signal in these organs derived from $Raptor^{D/D}$ mice (Extended Data Fig. 9m). Moreover, adeno-associated virus (AAV)-mediated depletion of *Nf2* or *Lats1/2* resulted in relatively more significant induction of mTORC1 signaling and liver mass in WT mice than $Raptor^{D/D}$ mice (Fig. 7d,e; Extended Data Fig. 9n,o). Due to the relatively low knockdown efficiency of *Lats1/2* in the heart (Extended Data Fig. 9n), we did not observe significant changes of heart mass of both WT and $Raptor^{D/D}$ mice following AAV injection (Extended Data Fig. 9o). These results collectively suggest that LATS1/2 controls organ size in part through suppressing mTORC1signaling by phosphorylating Raptor-S606.

## Discussion

Altogether, our study provides a mechanistic insight into a direct interplay between Hippo and mTORC1 pathways. When the Hippo pathway is active, Raptor is phosphorylated at S606 by the LATS1/2 kinase, leading to reduced binding with mTORC1 activator Rheb, thereby turning off mTORC1 signaling (Fig. 7f). On the other hand, when the Hippo pathway is inactive, Raptor remains unphosphorylated and interacts with Rheb, subsequently turning on mTORC1 to facilitate cell proliferation and cell growth (Fig. 7f). Therefore, our finding provides a possible molecular mechanism by which the temporal and spatial coordination between Hippo and mTOCR1 pathways dictates cell size and cell number to fine-tune organ and body development.

Previous study showed that YAP activates PI3K-mTOR pathway by inducing miR-29 levels to suppress PTEN translation in HeLa and MCF10A cells[17]. However, we found that LATS1/2-mediated phosphorylation of Raptor suppresses mTORC1 signaling independent of YAP/TAZ in our cell lines, such as HEK293 and MCF7 cells. Moreover, $Raptor^{D/D}$ mutation inhibited mTORC1 activity and size of certain organs in mice, including liver, heart and kidney. Therefore, our study suggest that in addition to YAP/TAZ, Raptor functions as another major downstream effector that mediates the effect of the Hippo pathway on controlling cell growth, proliferation and organ size. These findings also indicate

that Hippo controlling mTORC1 pathway may be in a cell type or tissue context-dependent manner, which is an interesting question and warranted a follow up study in the future.

## Methods

### Cell culture.

HEK293, HEK293T, HEK293E, MCF7, HeLa, HCT116, HEK293A and its derived cell lines were maintained in Dulbecco's Modified Eagle's Medium (DMEM) containing 10% fetal bovine serum (FBS), 100 units/ml penicillin and 100 μg/ml streptomycin. Cell transfection was performed as described previously[36]. Lentiviral shRNA virus packaging and subsequent infection of various cell lines were performed according to the protocol described previously[37]. Latrunculin B (Sigma, L5288), Forskolin (Sigma, F6886), Oleoyl-L-α-lysophosphatidic acid sodium salt (LPA. Sigma, L7260), Sphingosine 1-phosphate (S1P. Sigma, S9666), mTOR inhibitor Torin1 (TOCRIS, 4247), insulin (Life Technologies, 41400045) and IGF-1 (Millipore, GF138) were used at indicated doses.

### Plasmid construction.

HA-Raptor, HA-mTOR, HA-GβL, HA-Sin1, HA-Rictor, HA-DEPTOR, HA-Rheb, HA-YAP1, HA-LATS1 and HA-MST1 were constructed by cloning the corresponding cDNAs into pcDNA3-super-HA vector. Flag-Raptor, JNK1, JNK2, CaMKK1, CaMK2β, CaMK4, NEK6 and NEK7 were generated by cloning the corresponding cDNAs into pcDNA3-super-Flag vector. pCMV-GST-Raptor, pCMV-GST-LATS1 and pCMV-GST-Rheb were constructed by cloning the corresponding cDNAs into pCMV-GST mammalian expression vector. pbabe-HA-Raptor was generated by cloning the Raptor cDNAs into pbabe-hygro vector. The Raptor fragments, N, MH and WD40, were cloned into pcDNA3-super-Flag or pCMV-GST vector. pLenti-LATS1, pLenti-Rap2A and pLenti-HA-Rheb were generated by cloning the corresponding cDNAs into pLenti-hygro vector. GST-4E-BP1 and GST-Rheb were generated by cloning the corresponding cDNA into pGEX-4T-1 bacterial expression vector. The *NF2* sgRNAs (sg1-GGCGAGGTGGTGCGGCGTGA and sg2-GTCCATGGTGACGATCCTCA) were cloned into lentiCRISPR v2 (Addgene 52961). Flag-LATS1, Flag-MST1, Flag-DEPTOR, Flag-PRAS40, HA-GST-RagC, HA-GST-RagD, HA-GST-S6K1, pLJM1-FLAG-metap2, shYAP and shRheb constructs were purchased from Addgene. shRNAs targeting DEPTOR, TSC2, TAZ, JNK1, JNK2, CaMKK1, CaMK2β, CaMK4, NEK6 and NEK7 were purchased from Sigma-Aldrich. Raptor, LATS1-AA and Rheb mutants were generated using the QuikChange XL Site-Directed Mutagenesis Kit (Stratagene) according to the manufacturer's instructions. Details of plasmid constructions are provided upon request.

### Antibodies.

All antibodies were used at a 1:1,000 dilution in TBST buffer with 5% non-fat milk for western blotting. Anti-mTOR antibody (2972), anti-Raptor antibody (2280), anti-GβL antibody (3274), anti-phospho-Ser473-Akt antibody (4060), anti-Akt pan antibody (4691), anti-Akt1 antibody (2938), anti-phospho-Thr389-S6K antibody (9234), anti-S6K1 antibody (9202), anti-phospho-S6 (Ser235/236) antibody (4858), anti-phospho-S6 (Ser240/244) antibody (2215), anti-S6 antibody (2217), anti-phospho-4E-BP1 (Thr37/46) antibody

(2855), anti-phospho-4E-BP1 (Ser65) antibody (9451), anti-4E-BP1 antibody (9644), anti-phospho-YAP (Ser127) antibody (4911), anti-YAP antibody (14074), anti-LATS1 antibody (3477), anti-MST1 antibody (14946), anti-SAV1 (3507), anti-Merlin antibody (12888), anti-GST antibody (2625), anti-RagA antibody (4357), anti-RagC antibody (5466), anti-DEPTOR antibody (11816), anti-PRAS40 antibody (2691), anti-biotin (HRP conjugate, 5571), anti-TSC2 antibody (3990), anti-JNK2 antibody (9258), anti-CaMKII (pan) antibody (3362) and anti-CaMKIV antibody (4032) were purchased from Cell Signaling Technology. Anti-NEK6 antibody (ab133494) and anti-NEK7 antibody (ab133514) were purchased from abcam. Anti-Raptor antibody (A300–553A) for IP and anti-LATS2 antibody (A330–479A) were purchased from Bethyl Laboratories. Anti-HA antibody (sc-805), anti-JNK1 (sc-1648), anti-PTEN (sc-7974) and anti-LAMP2 (sc-18822) were purchased from Santa Cruz Biotechnology. Anti-tubulin antibody (T5168), polyclonal anti-Flag antibody (F7425), monoclonal anti-Flag antibody (F3165), anti-Flag agarose beads (A2220), anti-HA agarose beads (A2095), peroxidase-conjugated anti-mouse secondary antibody (A4416) and peroxidase-conjugated anti-rabbit secondary antibody (A4914) were purchased from Sigma. Monoclonal anti-HA antibody (901503) was purchased from Biolegend. Anti- CaMKK1 antibody was purchased from Novus Biologicals (NBP1–42683). Raptor-pS606 antibody was generated by Cell Signaling Technology.

### Immunoblot (IB) and immunoprecipitation (IP) analyses.

Cells were lysed in CHAPS buffer (40 mM HEPES pH 7.4, 2.5mM $MgCl_2$, 0.3% CHAPS) or EBC buffer (50 mM Tris pH 7.5, 120 mM NaCl, 0.5% NP-40) supplemented with protease inhibitors (Complete Mini, Roche) and phosphatase inhibitors (phosphatase inhibitor cocktail set I and II, Calbiochem). The cell lysates were clarified by centrifugation at 13,000 r.p.m. at 4 °C for 10 min. The protein concentrations of lysates were measured by the Beckman Coulter DU-800 spectrophotometer using the Bio-Rad protein assay reagent. Same amounts of whole cell lysates were resolved by SDS-PAGE and immunoblotted with indicated antibodies. For immunoprecipitation, 1000 μg lysates were incubated with 50% slurry of the affinity gel for 3 hours or the indicated antibody (1–2 μg) for 3–4 hours at 4 °C followed by one-hour incubation with Protein A sepharose beads (GE Healthcare). Immunoprecipitants were washed three times with CHAPS buffer containing 150 mM NaCl or NETN buffer (20 mM Tris, pH 8.0, 150 mM NaCl, 1 mM EDTA and 0.5% NP-40) before being resolved by SDS-PAGE.

### *In vitro* kinase assays.

*In vitro* mTORC1 kinase assays were performed as described previously[27]. Briefly, cells were lysed in ice-cold CHAPS buffer (40 mM HEPES [pH 7.4], 2 mM EDTA, 0.3% CHAPS) supplemented with protease inhibitors (Complete Mini, Roche) and phosphatase inhibitors (phosphatase inhibitor cocktail set I and II, Calbiochem). For immunoprecipitation, lysates were incubated with the indicated antibody (1–2 μg) for 2 hours at 4 °C followed by one-hour incubation with Protein A sepharose beads (GE Healthcare). Immunoprecipitates were washed four times with wash buffer (40 mM HEPES [pH 7.4], 2 mM EDTA, 150 mM NaCl, 0.3% CHAPS) and then washed twice with buffer 25 mM HEPES (pH 7.4), 20 mM KCl. The immunoprecipitates were then mixed with 0.5 μg bacterially purified GST-4E-BP1 as the substrate and incubated for 20 min at 30 °C in

mTORC1 kinase buffer (25 mM HEPES [pH 7.4], 50 mM KCl, 10 mM $MgCl_2$, 250 μM ATP). The kinase reaction was stopped by the addition of 3X SDS sample buffer and subsequent incubation at 95 °C for 5 min. The samples were analyzed by SDS-PAGE and immunoblotted with indicated antibodies. To observe Rheb-induced activation of mTORC1 complex, Rheb was added for 20 min before the addition of ATP.

For *in vitro* LATS1 kinase assays, full-length GST-Raptor protein purified from HEK293 cells was mixed with 200 ng active LATS1 kinase (Abcam, ab125612) in the kinase buffer (20 mM Tris-HCl [pH 7.5], 5mM $MgCl_2$, 5 mM $MnCl_2$, 2 mM DTT, 10 μM ATP, 5 μCi of [$\gamma-^{32}$P] ATP) and incubated at 30 °C for 30 min. The reaction was stopped by the addition of 3X SDS sample buffer and subsequent incubation at 95 °C for 5 min before analyzed by SDS-PAGE.

### Mass spectrometry analysis of Raptor S606 phosphorylation in cells.

293T cells were co-transfected with HA-Raptor and Flag-LATS1/MST1. 48 hours post-transfection, cells were harvested with EBC buffer and the whole-cell lysates were collected to perform HA immunoprecipitation. The HA immunoprecipitates were then resolved on SDS-PAGE and visualized by GelCode Blue Stain (Thermo Scientific, 24590). The band containing HA-Raptor was excised and digested with trypsin. The peptide mixture was analyzed by $C_{18}$ microcapillary liquid chromatography tandem mass spectrometry (LC-MS/MS) using a high-resolution hybrid Q Exactive HF Orbitrap mass spectrometer (Thermo Scientific) coupled to an EASY-nLC II nano-flow HPLC (Thermo Scientific) in positive ion mode. Higher collision energy (HCD) fragmentation spectra acquired by data dependent acquisition (DDA) in Top 8 mode were searched against the concatenated decoy Human protein database version 20171220 (UniProt) using the Mascot 2.5.1search engine. Data were interpreted and reported using Scaffold 4.6 and Scaffold PTM 33.1 software (Proteome Software). Peptides were accepted if they passed a 1.0% false discovery rate (FDR) threshold.

### Generation of CRISPR knock-in or knockout cell lines.

Generation of *Raptor* mutant cells was followed the protocol described previously[21]. The sgRNA (GGCGAGGTGGTGCGGCGTGA) targeting the genomic sequence near the Raptor S606 site were designed using the Zhang laboratory CRISPR design tool (http://crispr.mit.edu) and was cloned into GeneArt CRISPR nuclease vector with OFP reporter (Life Technologies, A21174). The 147-nt ssODN repair templates (desalted, IDT) were designed with homologous genomic flanking sequence centered around the S606 site and containing S606A or S606D mutation, as well as a silent change to the PAM site that does not alter the amino acid sequence. The S606A or S606D mutation removes the SfcI restriction enzyme site and results in that the PCR products were unable to cut by SfcI. The sgRNA construct and the ssODN were co-transfected into HEK293, 293E or HCT116 cells. 48 hours post-transfection, the OFP positive cells were enriched by FACS sorting with FITC channel and seeded into 96-well plate with one cell per well. Genomic DNA was extracted using the Quick Extract DNA Extraction Solution (Epicenter, Q09050) following the manufacturer's protocol. The genomic DNA fragment containing the S606 site was amplified by PCR and digested by SfcI (NEB, R0561) to screen for the potential correct

clones. Finally, successful knock-in mutant was verified by Sanger sequencing. The primers for amplification of the genomic DNA were forward, CTTCAGGGAAACCTCATTGC and reverse, CCAAGGTCCCACTGTCCTAC. ssODN for S606D, GCAGTCGGCAGCCAGGAGGACTGGACTCTGAGCCCCCGCCTGACTCACCTCGGG AATGGGGTCGGAGAGGAGGTCGTAGAGCTTCTCATGAGCGCTGTCTCTCACGCCG CACCATCTCGCCGAGTCGAAGTTCTGCCAGATCCTGCC. ssODNA for S606A, GCAGTCGGCAGCCAGGAGGACTGGACTCTGAGCCCCCGCCTGACTCACCTCGGG AATGGGGTCGGAGAGGAGGGCGTAGAGCTTCTCATGAGCGCTGTCTCTCACGCCG CACCACCTCGCCGAGTCGAAGTTCTGCCAGATCCTGCC.

To insert an N-terminal 3×Flag tag into the Raptor, the sgRNA (GCATTTCGGACTCCATCAGT) targeting the genomic sequence near the Raptor ATG codon were designed using the Zhang laboratory CRISPR design tool (http://crispr.mit.edu) and was cloned into lentiCRISPR v2 vector (Addgene, 52961). The sgRNA construct and single-strand DNA oligos were co-transfected into HEK293-S606D$^{knock\text{-}in}$ or S606A$^{knock\text{-}in}$ cells. 48 hours post-transfection, the transfected cells were trypsinized and cultured with medium containing 1 μg/ml puromycin for 48 hours. The alive cells were then seeded into 96-well plate with one cell per well. The knock-in cells were identified by PCR and Sanger sequencing. Genomic PCR primers: Raptor-N-Flag-F: TTTAAGGCTGGAGGTTCTCG and Raptor-N-Flag-R: AAAAGCCAAAGGTAGGTTCCAG. Single-strand DNA oligos: AGATCAGCCTCATCTTCCTCCCCCAGGCCCAGAAGAGGCGATTGCAGCATTTCGG ACT CGCCTGCGGCCGCCTTGTCATCGTCATCCTTGTAATCAATGTCATGATCTTTATAAT CACCGTCATGGTCTTTGTAGTCCATCAGTGGGGGAGGGGGTGGGGGAGTCCTTGG CAGCAAGCGCTCGAGAACCTCCAGCCTTAA.

### Immunofluorescence.

Cells grown on glass coverslips were fixed with 4% paraformaldehyde for 15 min at room temperature and then washed 3 times with PBS and permeabilized with 0.05% Triton X-100 for 10 min at room temperature. Following three 5 min washes in PBS, coverslips were blocked with 5% BSA for 30 min and then incubated with mTOR and LAMP2 antibodies overnight at 4 °C. Following three 5 min washes in PBST, coverslips were incubated with secondary antibodies, anti-rabbit Alexa Fluor 488 (Life Technologies/Molecular Probes), anti-mouse Alexa Fluor 594 (Life Technologies/Molecular Probes, A11032), for 1 hour at room temperature in the dark. Following three 5 min washes with PBST, coverslips were stained with DAPI and mounted ProLong Gold Antifade Mountant (Life Technologies/ Molecular Probes, P36930).

### Amino acid and serum starvation and stimulation.

For amino acid deprivation and stimulation experiments, sub-confluent cells were rinsed and incubated with amino acid-free DMEM (USBiological Life Sciences, D9800–13) for 50 min and then the media was replaced with standard DMEM (stimulated) or fresh amino-acid free DMEM (unstimulated) for 10 min. For insulin or IGF-1 stimulation, cells were serum starved for 16 hours and stimulated with 100 nM insulin or IGF-1 for indicated time.

### Colony formation assays.

Cells were seeded in 6-well plates (800 cells/well) and cultured for 8–12 days until formation of visible colonies. Colonies were fixed with 10% acetic acid/10% methanol for 20 min and then stained with 0.4% crystal violet/20% ethanol for 20 min. After staining, the plates were washed with distilled water and air-dried. The colonies were counted for statistic analysis.

### Soft agar assays.

The anchorage-independent cell growth assays were preformed in 6-well plates with the bottom layer containing 0.8% noble agar. $3x10^4$ cells were mixed with noble agar to final concentration of 0.4% and put on the top of bottom agar per well. The dishes were then cultured at 37 °C incubator for 3 weeks and 500 μl complete DMEM medium was added to keep the top layer moisture. The cells were stained with 1 mg/ml iodonitrotetrazolium chloride (sigma I10406) for colony visualization and counting.

### LC-MS/MS metabolomic profiling.

For metabolite extraction, triplicate 10 cm plates cells (60% confluent) were cultured for 16 hours. Medium was aspirated and 4 ml dry ice-cold 80% methanol was added immediately. The plates were then incubated for 10 min at −80 °C. Then, cells were collected and centrifuged at 5,000g for 5 min. The supernatant were transferred to a 1.5 ml tube and dried using a refrigerated SpeedVac. The extract was re-suspended in 20 μl HPLC-grade water just prior to the LC-MS analysis as described previously[38]. The data were analyzed using GENE-E software.

### Real-time RT-PCR analyses.

Total RNA was extracted using the RNeasy mini kit (Qiagen), and the reverse transcription reaction was performed using iScript™ Reverse Transcription Supermix (Bio-Rad, 1708841). Real-time RT-PCR analysis was performed using Power SYBR® Green PCR Master Mix (ABI, 4367659) with the 7500 Fast Real-time PCR system (ABI). Primers were listed in Supplementary Table 1.

### ECAR measurement.

Extracellular acidification rate (ECAR) is measured using Seahorse XF24 analyzer (Agilent Technologies, Santa Clara, CA). Briefly, $2x10^4$ cells were planted into gelatin-coated Seahorse microplate for 24 hours before analysis. On the day of analysis, the medium was changed to Seahorse XF basal media without glucose. The final concentrations of glucose, oligomycin, and 2-DG were 10 mM, 1 μM and 50 mM.

### Mouse xenograft assays.

$2x10^6$ indicated HCT116 cells were suspended using 100 μl of DMEM medium and injected into the flanks of female nude mice (NCRNU-M-M from Taconic, 4-5 weeks of age, 4 mice for each group). Tumor size was measured every 3 days with a caliper and the tumor volume was determined with the formula: $L \times W^2 \times 0.52$, where L is the longest diameter and W is

the shortest diameter. At the end of the studies, mice were sacrificed and *in vivo* solid tumors were dissected and weighed.

### Generation of *Raptor*$^{D/D}$ knock-in mice.

Cas9 protein (CP01) and sgRNAs were purchased from PNA Bio. ssDNA oligo (desalted, IDT) were designed with homologous genomic flanking sequence centered around the S606 site and containing S606D mutation, as well as a silent change to the PAM site that does not alter the amino acid sequence. sgRNAs (15 ng/ml) and ssDNA oligo (100 ng/ml) were mixed and injected into zygotes from the C57BL/6 female mice by the BIDMC Transgenic Core. sgRNA_1: CGACTCTGCAAGATGGTGTG. sgRNA_2: GGAGGCTATAGAGCTTTTCG. ssDNA oligo: CAATCTCTTTACAGATAAAACCCACCACCGCTCTGACCTAGCACAGAAGCTTACATCTGCAAGGACAACTCACCTCAGGGATGGGATCAGAGAGGAGGTCATAGAGCTTTTCGTGCGCA GTCTCTCACGCCACACCATCTTGCAGAGTCGAAGTTCTGCCAGATCCTTCCCAGGCAAATGGCCACCCACTGGCGTAGC. The mutant mouse was backcrossed with C57BL/6 mice for a minimum of two generations before carrying out experimental procedures. To verifiy the *Raptor*$^{D/D}$ knock-in mouse, PCR was performed with the primers mRaptor-S606-GT-F (TGCCCCACTTACCTATGTCC) and mRaptor-S606-GT-R (TAGCCTATCTTGGGGTCTGC). The PCR product was digested using SfcI restriction enzyme.

### Immunohistochemistry (IHC) analysis of mTORC1 signaling in mice.

Five weeks old mice were euthanized and indicated organs were collected. Small portions of the liver, heart, kidney, spleen and brain were fixed in formalin and processed for S6 pS235/S236 immunohistochemistry as described[39].

### Adeno-associated virus (AAV)-mediated knockdown of *Lats1/2* and knockout of *Nf2* in mice.

The conserved DNA sequence between mouse *Lats1* and *Lats2* genes was selected as the targets to design artificial microRNA. Synthesized gBlock harboring silencing RNAs against both mouse *Lats1* and *Lats2* was cloned into the intronic region of pAAVsc-CBPIEGFP plasmid[40]. The guide RNA targeting mouse *Nf2* (AGGAGGCCGAGCGTACAAGAG and AGAGGCTGAGCAAGAGATGCA) was cloned into pX602 AAV vector (Addgene, #61593). These AAV constructs were packaged into AAV8 by transient transfection of HEK293 cells and purified by Iodixanol gradient as previously described[41]. The vectors were titered by Q-PCR with BioRad CFX Connect using the EGFP primers (Forward 5'-AGAACGGCATCAAGGTGAAC-3' and Reverse 5'-GAACTCCAGCAGGACCATGT-3'). The AAV8 vectors were administered by tail vein injection of one month-old C57BL/6 or C57BL/6-derived *Raptor*$^{D/D}$ male mice at a dose of $1 \times 10^{11}$ vg/ mice in a total volume of 200 μl. 4 weeks or 8 weeks post the injection, mice were euthanized and organs were weighed.

All mouse experiments were conducted under the protocol (Protocol #043–2015) approved by Institutional Animal Care and Use Committee (IACUC, RN150D) at Beth Israel

Deaconess Medical Center (BIDMC). The Institute is committed to the highest ethical standards of care for animals used for the purpose of continued progress in the field of human cancer research. All mice were housed in a pathogen-free environment at BIDMC animal facility and were handled in strict accordance with the “Guide for the Care and Use of Laboratory Animals” and the applicable institutional regulations.

### Statistics and reproducibility.

The in vitro experiments were repeated at least three times unless stated otherwise. As indicated in the figure legends, all quantitative data were presented as mean ± s.d or mean ± s.e.m of three biologically independent experiments or samples. Statistical analyses were performed using GraphPad Prism 7 and Excel. Statistical significance was tested using two-tail unpaired or paired Student’s t-test. A $P$ value less than 0.05 was considered significant.

### Data availability.

All data that support the findings of this study are available on request from the corresponding author.

## Extended Data

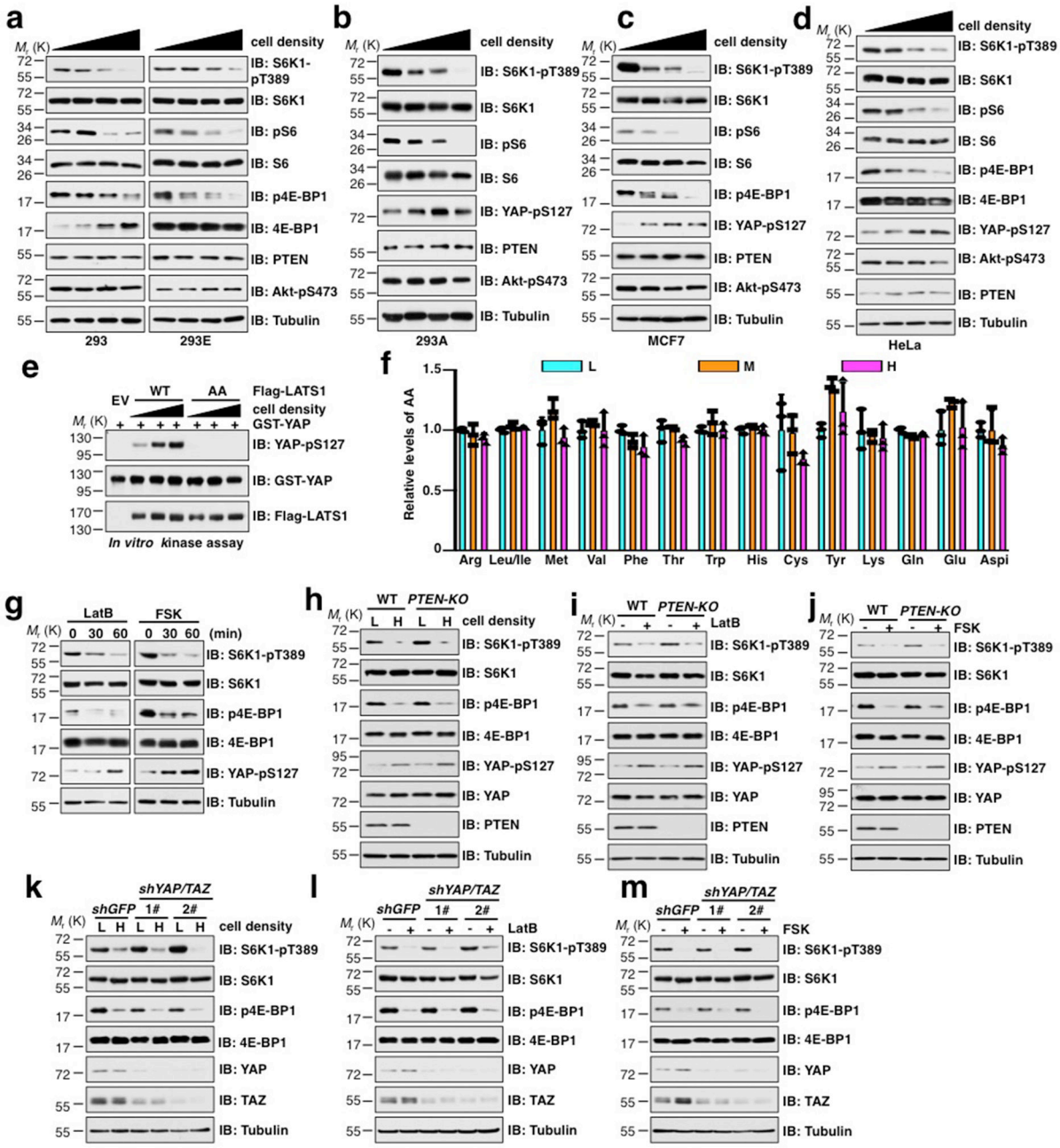


**Extended Data Fig. 1. Activation of the Hippo pathway negatively regulates mTORC1 kinase activity independent of YAP/PTEN.**

**a-d.** 293, 293E (a), 293A (b), MCF7 (c) and HeLa (d) cells were cultured in 60 mm dishes at 25%, 50%, 75% and 100% confluence for 16 hours before harvesting for immunoblot (IB) analysis. **e.** Increasing cell density activates LATS1 *in vitro*. IB analysis of LATS1 *in vitro* kinase assay samples. **f.** 293 cells were seeded on 60 mm dishes at 30% (L), 60% (M) and 100% (H) confluence for 16 hours and then replaced with fresh medium for 1 hour. The media was collected for Mass spectrometry analysis of relative amino acid (AA) levels. Data were shown as mean ± s.d. of n=3 biological independent samples. **g.** IB analysis of whole cell lysates (WCL) derived from 293 cells treated with 1 μg/ml LatB or 10 μM Forskolin

(FSK) for indicated time. **h.** 293 wild type (WT) and *PTEN* knockout (*PTEN*-KO) cells were cultured in 60 mm dishes at 30% (L) and 100% (H) confluence for 16 hours before harvesting for IB analysis. **i-j.** IB analysis of WCL derived from 293-WT and *PTEN* knockout (*PTEN*-KO) 293 cells treated with 1 μg/ml LatB or 10 μM Forskolin (FSK) for 60 min. **k-m.** 293 cells were infected with lenti-viral sh*YAP* and sh*TAZ* vectors and then selected with 1 μg/ml puromycin for 72 hours to eliminate the non-infected cells. The resulting cells were cultured in 60 mm dishes at 30% (L) and 100% (H) confluence for 16 hours (k) or treated with 1 μg/ml LatB (l) or 10 μM Forskolin (FSK) (m) for 60 min before harvesting for IB analysis. Western blots in **a-e** and **g-m** were performed n=2 independent experiments, with similar results obtained.

Unprocessed immunoblots are shown in Source Data Extended data Fig. 1. Statistical source data are available in Statistical Source Data Extended Data Fig. 1.

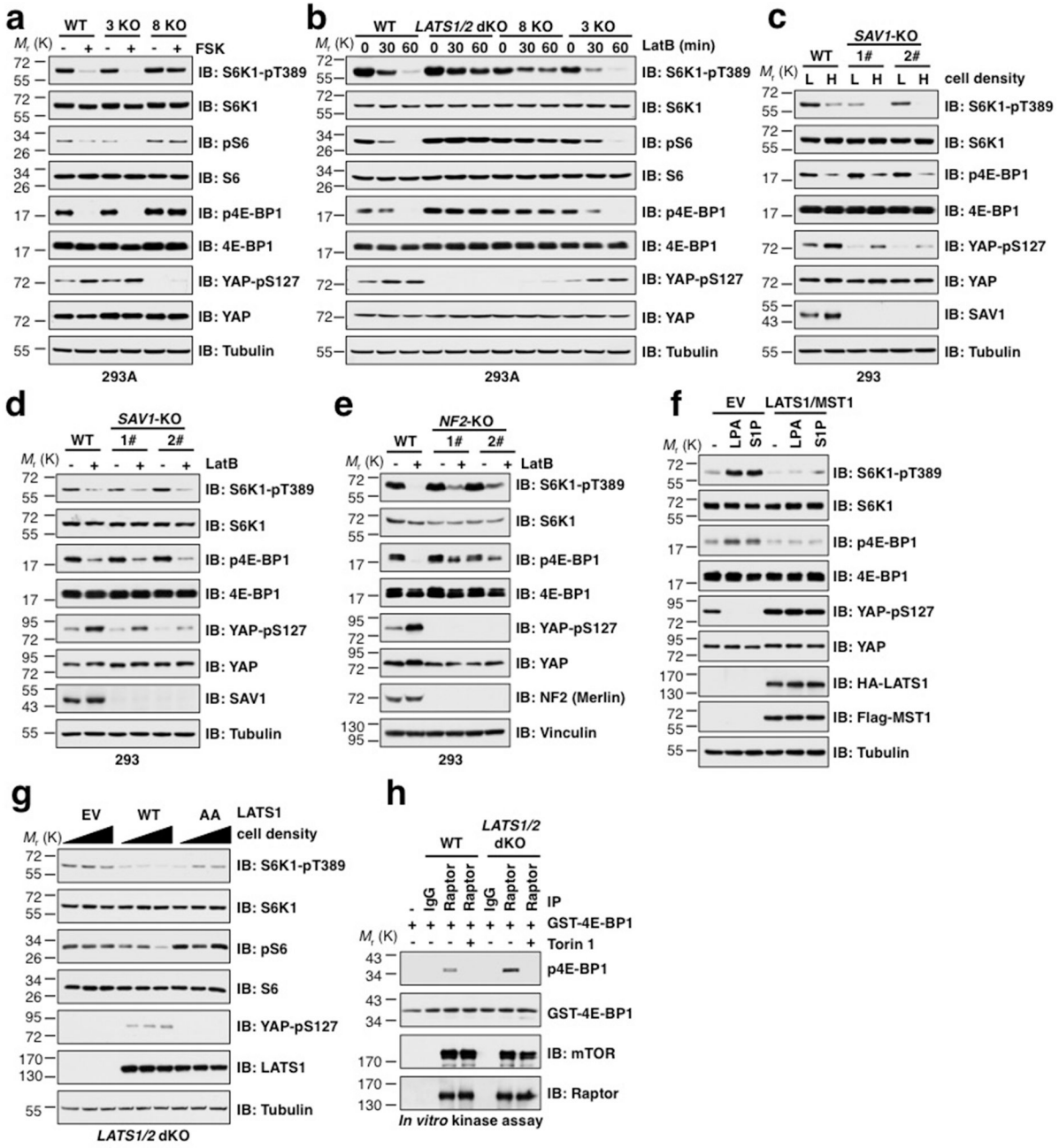


**Extended Data Fig. 2. The Hippo pathway suppresses mTORC1 signaling depending on LATS1/2 kinase activity.**

**a-b.** IB analysis of whole cell lysates (WCL) derived from 293A-WT, *MAP4K4/6/7* (3 KO) and *MAP4K1/2/3/4/6/7 MST1/2* (8 KO) cells treated with 10 μM Forskolin (FSK) (a) or 1 μg/ml LatB (b) for 60 min. **c-d.** IB analysis of WCL derived from 293-WT and *SAV1*-KO cells at 30% (L) and 100% (H) confluence (c) or treated with 1 μg/ml LatB (d) for 60 min. **e.** IB analysis of WCL derived from 293-WT and *NF2*-KO cells treated with 1 μg/ml LatB for 60 min. **f.** IB analysis of WCL derived from 293 cells transfected with LATS1/MST1 or EV (as a negative control). The cells were treated with 1 μM LPA or 1 μM S1P for 60 min before harvesting. **g.** *LATS1/2* dKO cells were infected with EV, WT-LATS1 or kinase-dead

LATS1 (AA) vector and selected with 200 μg/ml hygromycin for 72 hours to eliminate the non-infected cells. The resulting cells were cultured in 60 mm dishes at 30%, 60% and 100% confluence and harvested for IB analysis. **h.** *In vitro* kinase assays demonstrate that genetic deletion of *LATS1/2* leads to increased mTORC1 kinase activity *in vitro* towards phosphorylating bacterially purified 4E-BP1. Raptor immunoprecipitates (IP) were prepared from 293A-WT or *LATS1/2* dKO cells and used for examination of mTORC1 kinase activity *in vitro*. 250 nM mTOR inhibitor Torin 1 was added as indicated. Western blots in **a-h** were performed n=2 independent experiments, with similar results obtained. Unprocessed immunoblots are shown in Source Data Extended data Fig. 2.

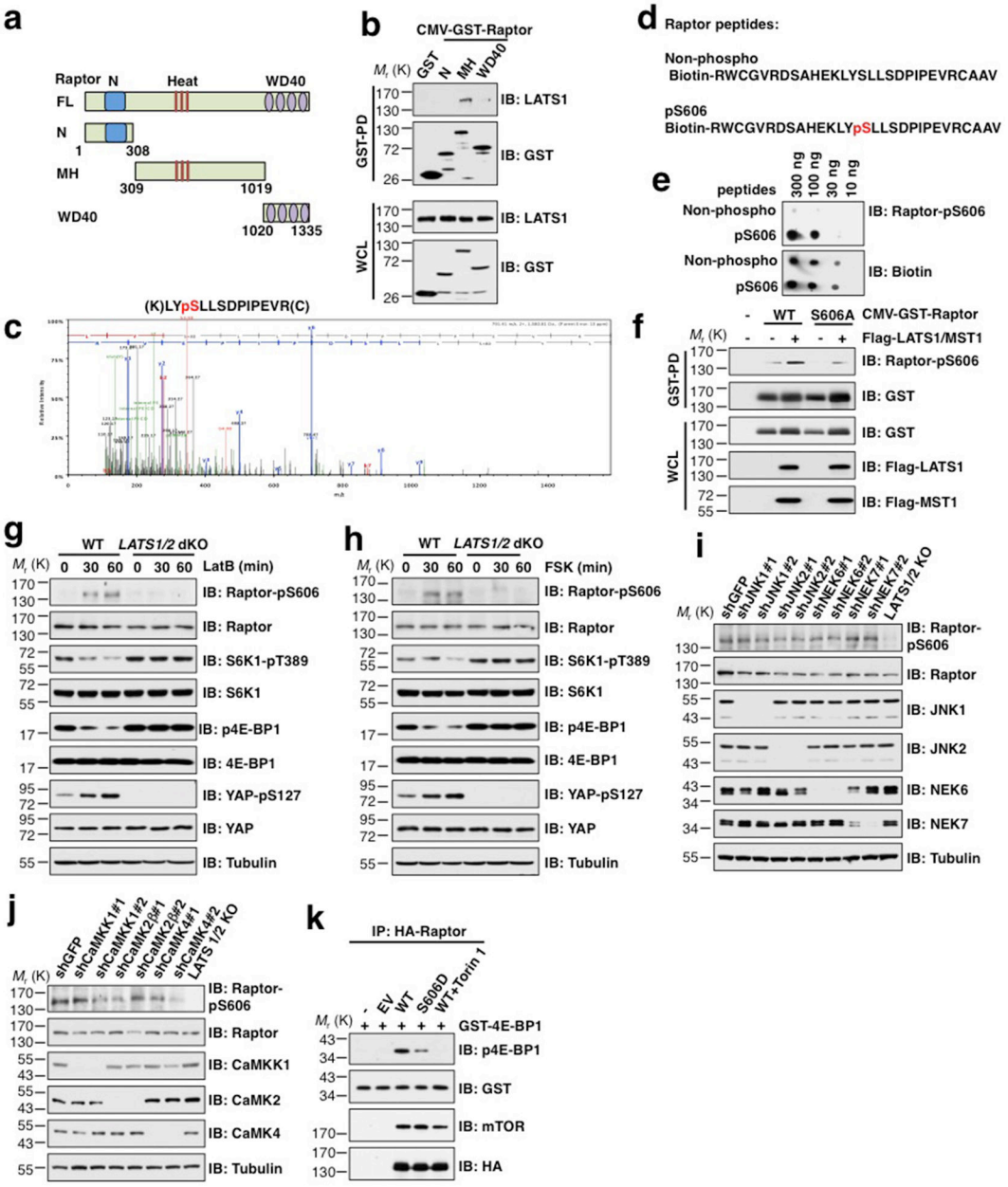


**Extended Data Fig. 3. LATS1/2 interacts with and phosphorylates Raptor at S606.**

**a.** A schematic illustration of the Raptor domain structures. **b.** The MH domain of Raptor interacts with endogenous LATS1. IB analysis of WCL and GST pull-down (GST-PD) products derived from 293 cells transfected with indicated constructs. **c.** The MS/MS fragmentation spectrum showing distinct **b-** (N-terminal) and **y-** (C-terminal) series fragment ions for the Raptor peptide LY**pS**LLSDPIPEVR defining the pSer606 site. This experiment was performed one time. **d.** Protein sequence illustration of synthesized Raptor peptides. **e.** Titration of the indicated Raptor peptides with or without S606 phosphorylation demonstrated that the generated Raptor-pS606 antibody specifically recognizes the pS606 epitope. **f.** S606A mutation blocks LATS1-mediated Raptor-S606 phosphorylation. IB analysis of WCL and IP derived from 293 cells transfected with indicated constructs. **g-h.**

*LATS1/2* dKO blocks Raptor-S606 phosphorylation. IB analysis of WCL derived from 293-WT, *LATS1/2* dKO cells treated with 1 μg/ml LatB (g) or 10 μM Forskolin (FSK) (h) for 60 min. **i-j.** LATS is the major kinase phosphorylating Raptor at S606. 293 cells were infected with lenti-viral vectors targeting indicated kinases and then selected with 1 μg/ml puromycin for 72 hours to eliminate the non-infected cells. *LATS1/2* KO cells as a positive control. **k.** S606D mutation decreases mTORC1 kinase activity *in vitro*. HA-Raptor IP were prepared from 293 cells and used for examination of mTORC1 kinase activity. 250 nM mTOR inhibitor Torin 1 was added as indicated. Western blots in **b** and **e-k** were performed n=2 independent experiments, with similar results obtained.
Unprocessed immunoblots are shown in Source Data Extended data Fig. 3.

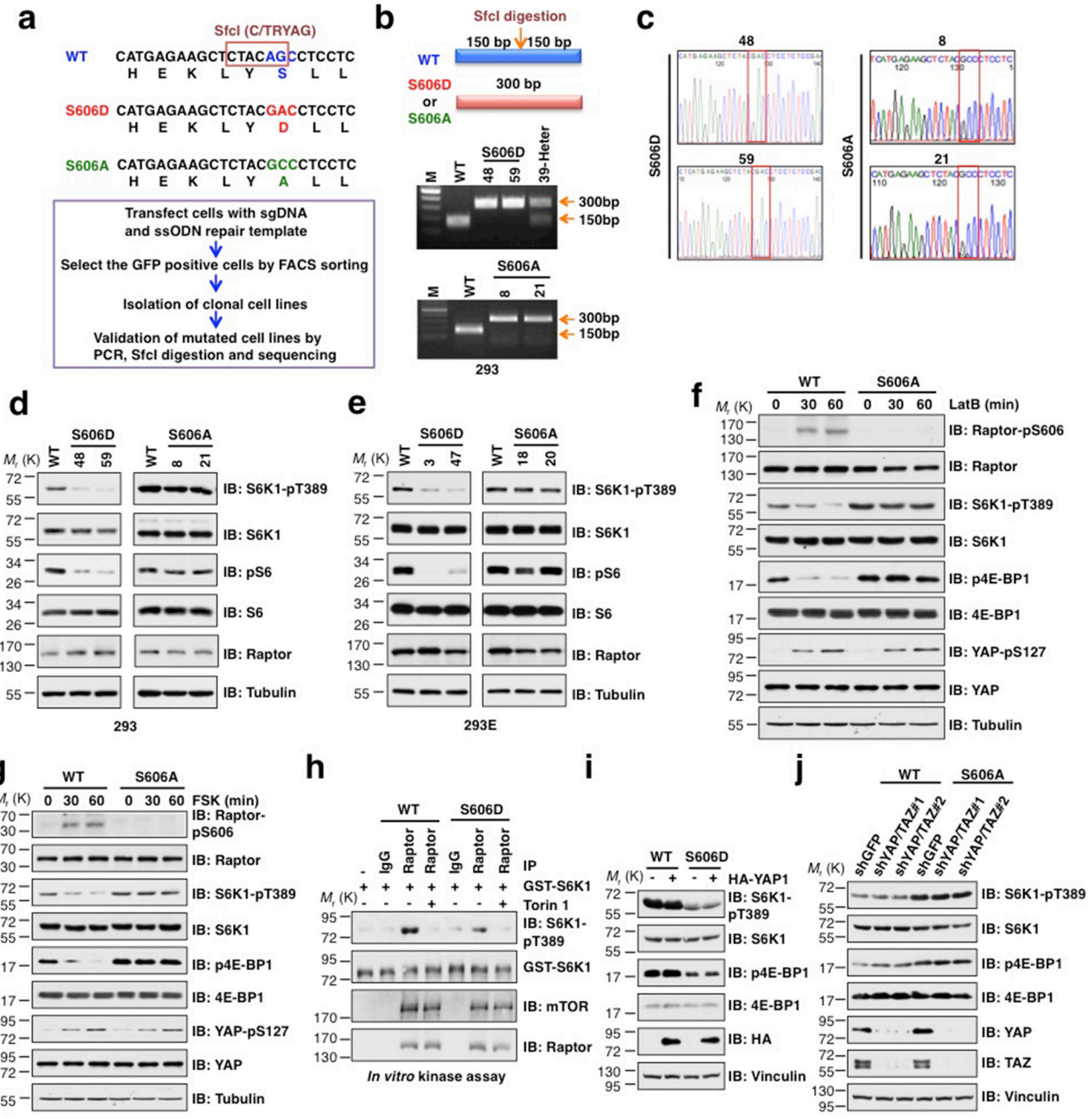


**Extended Data Fig. 4. Generation of Raptor S606D$^{knock\text{-}in}$ and S606A$^{knock\text{-}in}$ cells by CRISPR.**

**a.** A schematic representation of the amino sequence and strategy to generate Raptor-S606D and S606A CRISPR knock-in cells. **b.** Identification of the potential knock-in mutants. Genomic DNA containing Raptor-S606D or S606A mutation were amplified by PCR and digested with SfcI. The experiment was repeated three times independently, with similar results obtained. **c.** Confirmation of the correct mutation of Raptor-S606D or S606A by Sanger DNA sequencing. **d-e.** S606Dknock-in cells display reduced mTORC1 activity. Immunoblot (IB) cell lysates (WCL) derived from 293 (d) and 293E (e) S606Dknock-in and S606Aknock-in cells. **f-g.** The S606A mutation largely blocks LatB or FSK-induced Raptor-

pS606. IB analysis of WCL derived from 293 knock-in cells treated with 1 μg/ml LatB (f) or 10 μM FSK (g) for indicted time periods. **h.** In vitro kinase assays shows that the S606D mutation reduces mTORC1 kinase activity in vitro towards phosphorylating S6K1. Raptor immunoprecipitates (IP) derived from 293-WT or S606Dknock-in cells were analyzed for mTORC1 kinase activity. 250 nM mTOR inhibitor Torin1 was added as indicated. **i.** IB analysis of WCL derived from 293-WT and S606Dknock-in cells transfected with HA-YAP1. **j.** IB analysis of WCL derived from 293-WT and S606Aknock-in cells infected with shYAP/TAZ virus. Western blots in d-j were performed n=2 independent experiments, with similar results obtained.

Unprocessed immunoblots are shown in Source Data Extended data Fig. 4.

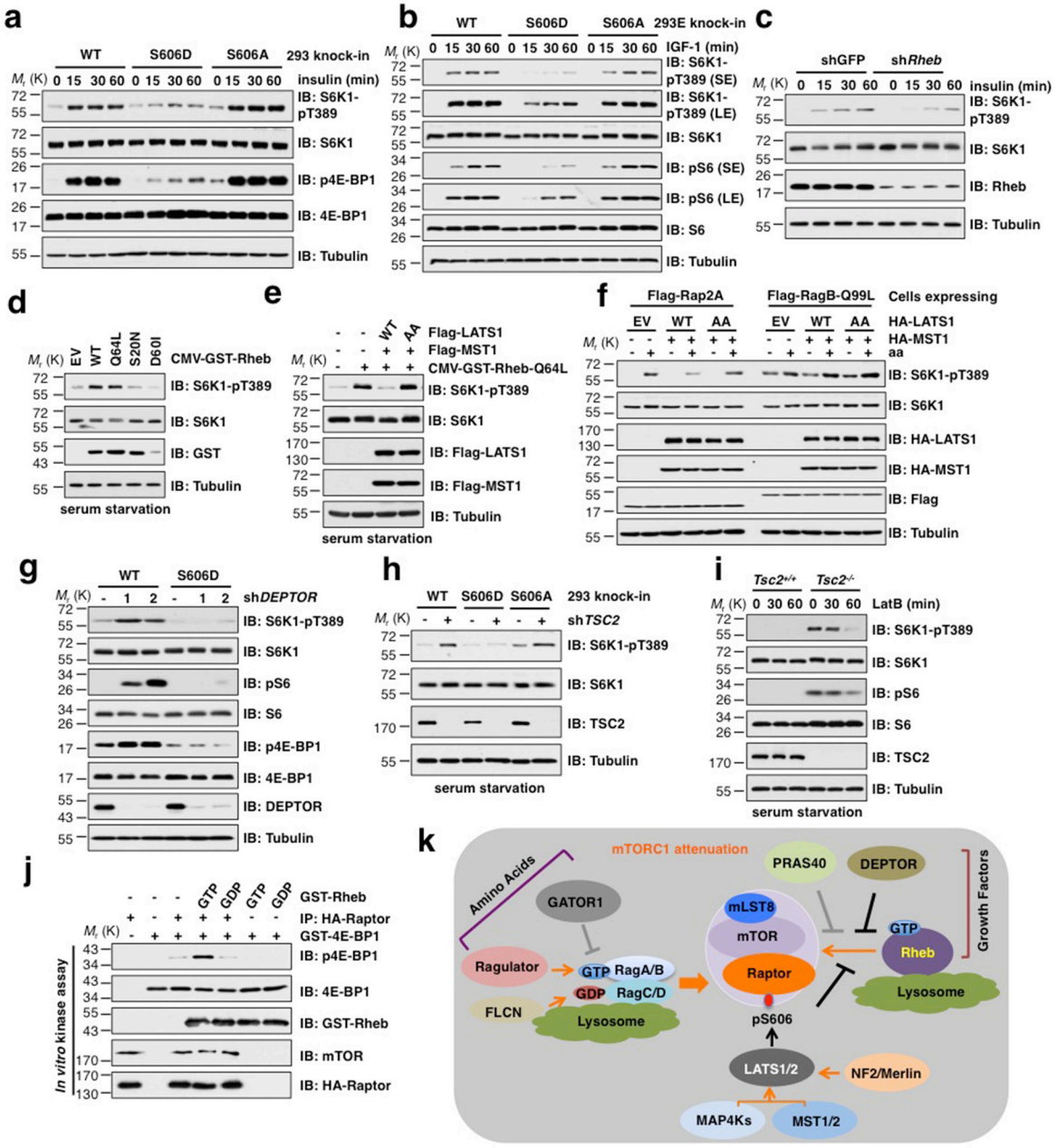


**Extended Data Fig. 5. LATS1 suppresses Rheb- and growth factor-induced mTORC1 activation.**

**a-b.** Growth factors induced-activation of mTORC1 is impaired in S606D$^{knock\text{-}in}$ cells. IB analysis of WCL derived from 293 or 293E cells treated with 100 nM insulin (a) or 100 ng/ml IGF-1 (b). **c.** IB analysis of WCL derived from *Rheb*-depleted 293 cells treated with 100 nM insulin. Cells were serum-starved for 16 hours before insulin stimulation. **d.** Rheb-WT and the GTP-bound mutant Q64L activate mTORC1 *in vivo*. IB analysis of WCL derived from 293 cells transfected with indicated Rheb constructs. **e.** LATS1-WT inhibits Rheb-induced activation of mTORC1. IB analysis of WCL derived from 293 cells transfected with indicated constructs. **f.** LATS1 does not affect RagB-induced activation of mTORC1. IB analysis of WCL derived from Rap2a or RagB-Q99L expressing 293 cells

transfected with indicated constructs. **g.** Depletion of *DEPTOR* cannot restore mTORC1 activity in S606D$^{knock\text{-}in}$ cells. IB analysis of WCL derived from 293E-WT and S606D$^{knock\text{-}in}$ cells infected with lentiviral sh*DEPTOR* vectors. **h.** The S606D mutation inhibits mTORC1 activation in *TSC2*-depleted cells under serum-starved condition. IB analysis of WCL derived from 293E-WT, S606D$^{knock\text{-}in}$ and S606A$^{knock\text{-}in}$ cells infected with lentiviral sh*TSC2* vector. Cells were serum-starved for 16 hours before harvesting. **i.** LatB suppresses *Tsc2*-loss-induced mTORC1 activation. IB analysis of WCL derived from *Tsc2*$^{+/+}$ and *Tsc2*$^{-/-}$ MEFs treated with 1 μg/ml LatB for indicated time period under serum-starved condition. **j.** Rheb activates mTORC1 *in vitro* in a GTP loading-dependent manner. HA-Raptor immunoprecipitates derived from 293 cells were analyzed for mTORC1 kinase activity toward 4E-BP1 in the presence of GTP- or GDP-bound Rheb. **k.** A proposed model to describe mechanistically how LATS1/2-mediated Raptor-S606 phosphorylation inhibits growth factors-induced mTORC1 activation. Western blots in **a-j** were performed n=2 independent experiments, with similar results obtained.

Unprocessed immunoblots are shown in Source Data Extended data Fig. 5.

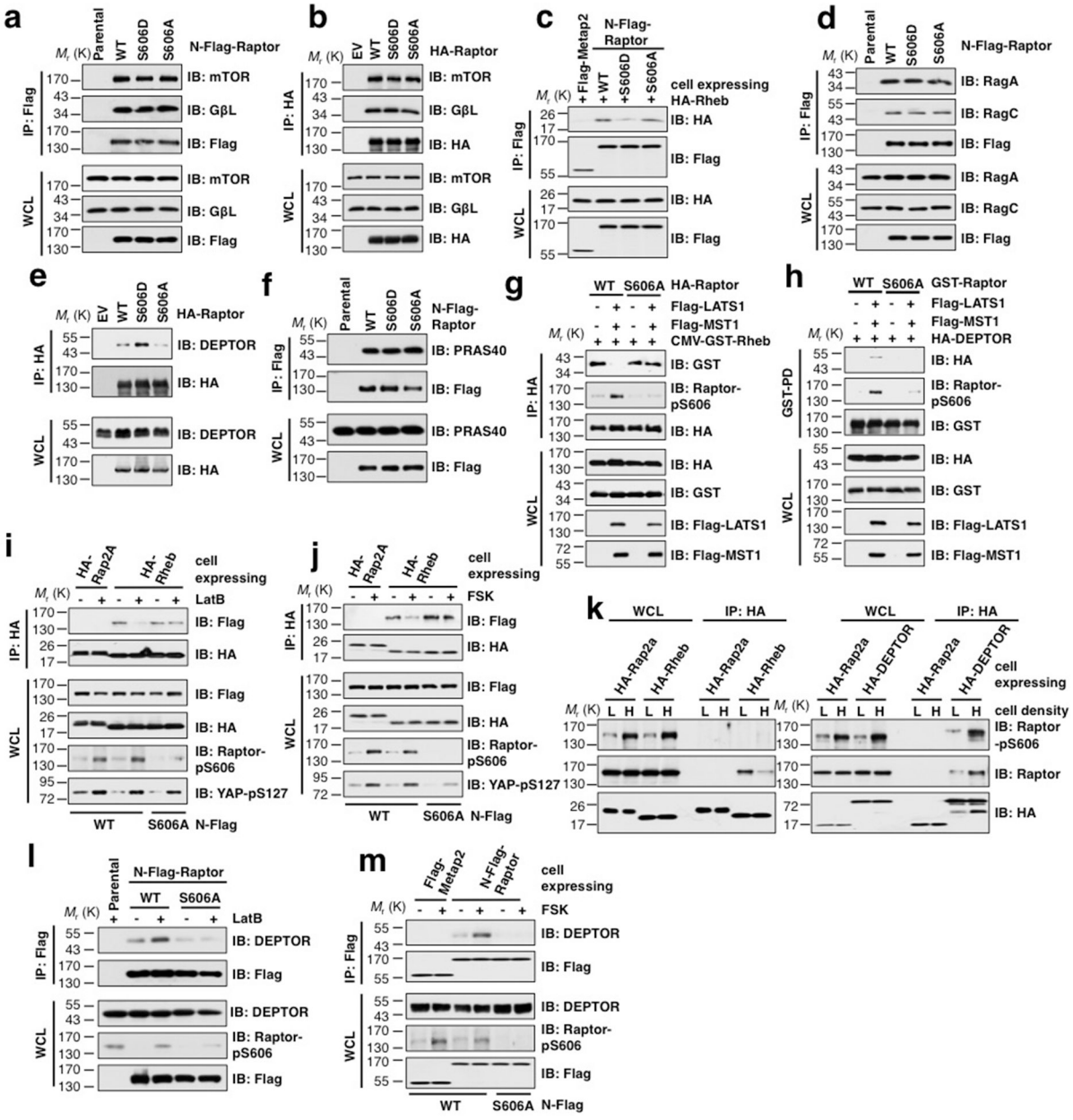


**Extended Data Fig. 6. The Raptor-S606D mutation affects its interaction with Rheb and DEPTOR in a LATS-dependent manner.**

**a-b.** The Raptor-S606D mutation does not affect mTORC1 complex formation. IB analysis of WCL and IP derived from 293 CRISPR knock-in cells (a) or 293 cells transfected with indicated constructs (b). **c.** The S606D mutation impairs its interaction with Rheb. IB analysis of WCL and IP derived from indicated CRISPR knock-in cells expressing HA-tag Rheb. **d.** The Raptor-S606D mutation does not affect its interaction with Rag GTPases. IB analysis of WCL and IP derived from indicated 293 CRISPR knock-in cells. **e.** The Raptor-S606D mutation increases its interaction with DEPTOR. IB analysis of WCL and IP derived from 293 cells transfected with indicated constructs. **f.** The Raptor-S606D mutation minimally affects its interaction with PRAS40. IB analysis of WCL and IP derived from

indicated 293 CRISPR knock-in cells. **g.** IB analysis of WCL and IP derived from 293 cells transfected with indicated constructs. **h.** IB analysis of WCL and GST pull-down products (GST-PD) derived from 293 cells transfected with indicated constructs. **i-j.** IB analysis of WCL and IP derived from indicated 293 CRISPR knock-in cells stably expressing HA-Rap2A (as a control) or HA-Rheb. The cells were treated with 1 μg/ml LatB (i) or 10 μM FSK (j) for 60 min before harvesting. **k.** IB analysis of WCL and IP derived from 293 cells stably expressing HA-Rheb or HA-DEPTOR cultured at low (30%) or high (100%) cell density. **l-m.** IB analysis of WCL and IP derived from indicated 293 CRISPR knock-in cells. The cells were treated with 1 μg/ml LatB (l) or 10 μM FSK (m) for 60 min before harvesting. Western blots in **a-m** were performed n=2 independent experiments, with similar results obtained.

Unprocessed immunoblots are shown in Source Data Extended data Fig. 6.

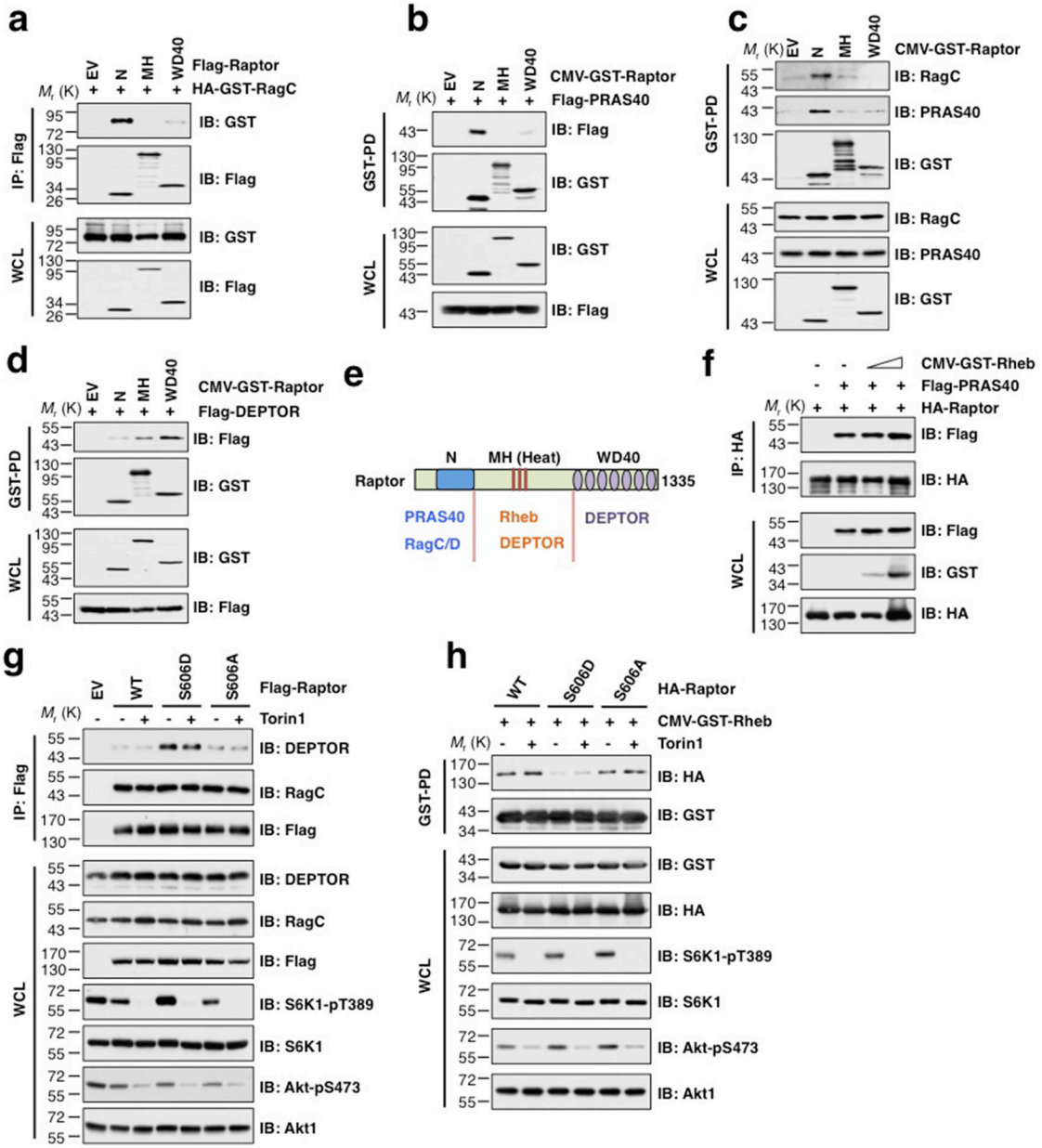


**Extended Data Fig. 7. Rag GTPases, PRAS40, Rheb and DEPTOR bind different domains of Raptor.**

**a-c.** Rag GTPases and PRAS40 interact with Raptor N-terminus. Immunoblot (IB) analysis of whole cell lysates (WCL) and immunoprecipitates (IP) derived from 293 cells transfected with indicated constructs. **d.** DEPTOR binds the MH domain and C-terminus of Raptor. IB analysis of WCL and IP derived from 293 cells transfected with indicated constructs. **e.** A schematic representation of the indicated domains of Raptor and a summary of each domain that is responsible for binding different Raptor-interacting proteins. **f.** Rheb does not affect the interaction between Raptor and PRAS40. IB analysis of WCL and IP derived from 293 cells transfected with indicated constructs. **g-h.** IB analysis of WCL and IP derived from 293 cells transfected with indicated constructs. Where indicated, cells were treated with 10 nM

mTOR inhibitor Torin 1 for 1 hour before harvesting. Western blots in **a-d** and **f-h** were performed n=2 independent experiments, with similar results obtained.
Unprocessed immunoblots are shown in Source Data Extended data Fig. 7.

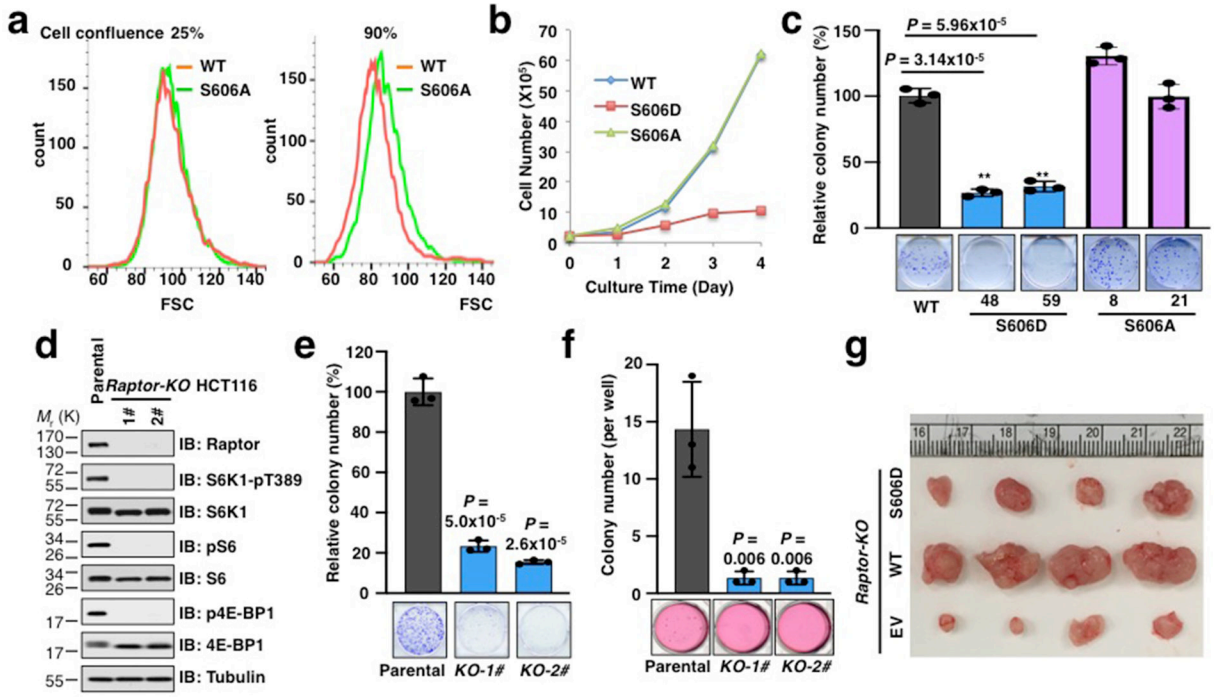


**Extended Data Fig. 8. The Raptor S606D mutation inhibits cell proliferation, colony formation and tumorigenesis.**

**a.** S606A$^{knock\text{-}in}$ cells display bigger cell size than WT cells at high cell confluence. Cells were grown in 10% serum at 25% or 90% confluence and subjected to cell size analysis by FACS. **b.** Growth curve of 293-WT, S606D$^{knock\text{-}in}$ and S606A$^{knock\text{-}in}$ cells to show that S606D$^{knock\text{-}in}$ cells proliferate slowly compared with WT and S606A$^{knock\text{-}in}$ cells. **c.** S606D$^{knock\text{-}in}$ cells, but not S606A$^{knock\text{-}in}$ cells, display reduced colony formation ability. Data were shown as mean ± SD of three independent experiments. *P* values were calculated using two-tailed Student's t-test. **d.** IB analysis of WCL derived from parental and *Raptor* knockout (*Raptor-KO*) cells. Blot is representative of two independent experiments, with similar results obtained. **e-f.** Colony formation assays (e) and soft agar assays (f) demonstrate the deficiency of *Raptor-KO* cells on cell transforming ability. Data were shown as mean ± SD of three independent experiments. *P* values were calculated using two-tailed Student's t-test. **g.** Tumors derived from xenograft assay in were dissected (n = 4 mice). Unprocessed immunoblots are shown in Source Data Extended data Fig. 8. Statistical source data are available in Statistical Source Data Extended Data Fig. 8.

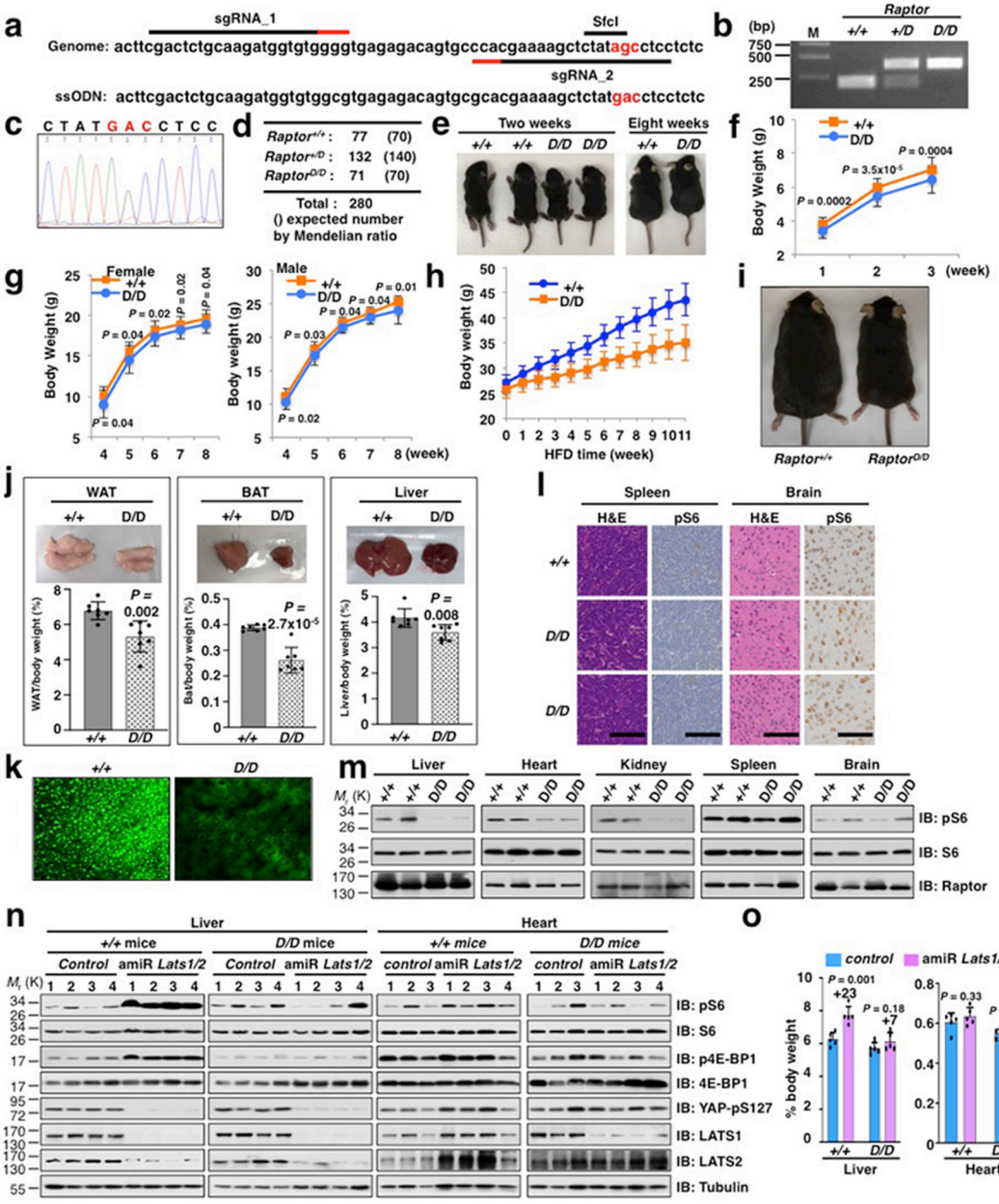


**Extended Data Fig. 9. Generation and characterization of *Raptor*$^{D/D}$ knock-in mice.**

**a.** sgRNA sequence and part of ssODN sequence used for generating *Raptor*$^{D/D}$ mice. **b.** Analysis of mouse genomic DNA by SfcI digestion. **c.** Sanger sequencing results of *Raptor*$^{D/D}$ mouse genomic DNA. **d.** Frequency of genotypes produced from *Raptor*$^{+/D}$ mouse intercrosses. **e.** Representative images of 2-week-old and 8 week-old mice. **f.** Body weight of mice. Data were shown as mean ± s.e.m. (n = 44 mice/group). **g.** Growth of female and male mice. Data were shown as mean ± s.e.m. (female, n = 20 mice/group; male, n = 18 mice/group). **h.** Body weight of mice fed with high fat diet (HFD). Data were shown as mean ± s.e.m. (n = 7 mice/group). **i.** Representative images of *Raptor*$^{+/+}$ and *Raptor*$^{D/D}$ mice fed with HFD for 11 weeks. **j.** Weight of white adipose tissue (WAT), brown adipose tissue (BAT) and liver was shown as percentage of body weight in mice that were on an HFD for

11 weeks. Data were shown as mean ± s.e.m. (n = 7/group). **k.** Representative image of bodipy staining of liver sections from *Raptor*$^{+/+}$ and *Raptor*$^{D/D}$ mice that were on an HFD for 11 weeks. **l.** Organ sections were analyzed by immunohistochemistry for pS6 (pS235/S236) levels. Scale bars, 50 μm for spleen and 100 μm for brain. **m.** IB analysis of WCL derived from indicated organs. **n.** IB analysis of WCL derived from livers and hearts of mice depleted Lats1/2. **o.** AAV-mediated knockdown of Lats1/2 increases liver size. Data were shown as mean ± s.e.m. (n = 5 mice/group). P values in f, g, j and o were calculated using two-tailed Student's t-test. The experiments in b, l, m and n were repeated n=2 independent experiments, with similar results obtained.

Unprocessed immunoblots are shown in Source Data Extended data Fig. 9. Statistical source data are available in Statistical Source Data Extended Data Fig. 9.

## Supplementary Material

Refer to Web version on PubMed Central for supplementary material.

## Acknowledgments

We thank Brian North, Bin Wang, Fabin Dang, Cong Jiang, Yang Gao, Naoe Taira Nihira, Kouhei Shimizu, Hiroyuki Inuzuka, Jinfang Zhang and other Wei laboratory members for critical reading and discussion of the manuscript. We also thank Dr. Brendan Manning (Harvard T. H. Chan School of Public Health, USA) for helpful suggestions and providing 293E cells, 4E-BP1 construct and LAMP2 antibody. *LATS1/2*-dKO, *MST1/2*-dKO, *MAP4K4/6/7*-3KO and *MAP4K1/2/3/4/6/7MST1/2*-8KO 293A cells were gift of Kun-Liang Guan (UC San Diego, USA). X.D. and J.G. were supported by NRSA T-32 training grants. P.L. is in part supported by R00CA181342 from National Cancer Institute. Y.L. and Y.Y. are supported by NCI grant R01CA222571. The AAV virus work was partially supported by NIH grant P30EY012196. The LC-MS/MS work was partially supported by NIH grants P01CA120964 (J.A.) and P30CA006516 (J.A.). The remainder work was supported in part by pilot funding from the MUSC Digestive Diseases Research Core Center Pilot & Feasibility Program (W.G.) and the NIH grants [R00CA207867 (W.G.), R01GM094777 (W.W.) and R01CA177910 (W.W.)].

## References

1. Conlon I & Raff M Size control in animal development. Cell 96, 235–244 (1999). [PubMed: 9988218]
2. Dong J et al. Elucidation of a universal size-control mechanism in Drosophila and mammals. Cell 130, 1120–1133 (2007). [PubMed: 17889654]
3. Wullschleger S, Loewith R & Hall MN TOR signaling in growth and metabolism. Cell 124, 471–484 (2006). [PubMed: 16469695]
4. Pan D Hippo signaling in organ size control. Genes & development 21, 886–897 (2007). [PubMed: 17437995]
5. Laplante M & Sabatini DM mTOR signaling in growth control and disease. Cell 149, 274–293 (2012). [PubMed: 22500797]
6. Tumaneng K, Russell RC & Guan KL Organ size control by Hippo and TOR pathways. Current biology : CB 22, R368–379 (2012). [PubMed: 22575479]
7. Yu FX, Zhao B & Guan KL Hippo Pathway in Organ Size Control, Tissue Homeostasis, and Cancer. Cell 163, 811–828 (2015). [PubMed: 26544935]
8. Pan D The hippo signaling pathway in development and cancer. Developmental cell 19, 491–505 (2010). [PubMed: 20951342]
9. Yu FX & Guan KL The Hippo pathway: regulators and regulations. Genes & development 27, 355–371 (2013). [PubMed: 23431053]
10. Meng Z, Moroishi T & Guan KL Mechanisms of Hippo pathway regulation. Genes & development 30, 1–17 (2016). [PubMed: 26728553]

11. Ma S, Meng Z, Chen R & Guan KL The Hippo Pathway: Biology and Pathophysiology. Annu Rev Biochem 88, 577–604 (2019). [PubMed: 30566373]
12. Zoncu R, Efeyan A & Sabatini DM mTOR: from growth signal integration to cancer, diabetes and ageing. Nature reviews. Molecular cell biology 12, 21–35 (2011). [PubMed: 21157483]
13. Saxton RA & Sabatini DM mTOR Signaling in Growth, Metabolism, and Disease. Cell 168, 960–976 (2017). [PubMed: 28283069]
14. Kim J & Guan KL mTOR as a central hub of nutrient signalling and cell growth. Nature cell biology 21, 63–71 (2019). [PubMed: 30602761]
15. Zhao B et al. Inactivation of YAP oncoprotein by the Hippo pathway is involved in cell contact inhibition and tissue growth control. Genes & development 21, 2747–2761 (2007). [PubMed: 17974916]
16. Yu FX et al. Regulation of the Hippo-YAP pathway by G-protein-coupled receptor signaling. Cell 150, 780–791 (2012). [PubMed: 22863277]
17. Tumaneng K et al. YAP mediates crosstalk between the Hippo and PI(3)K-TOR pathways by suppressing PTEN via miR-29. Nature cell biology 14, 1322–1329 (2012). [PubMed: 23143395]
18. Hamaratoglu F et al. The tumour-suppressor genes NF2/Merlin and Expanded act through Hippo signalling to regulate cell proliferation and apoptosis. Nature cell biology 8, 27–36 (2006). [PubMed: 16341207]
19. Zhang N et al. The Merlin/NF2 tumor suppressor functions through the YAP oncoprotein to regulate tissue homeostasis in mammals. Developmental cell 19, 27–38 (2010). [PubMed: 20643348]
20. Yin F et al. Spatial organization of Hippo signaling at the plasma membrane mediated by the tumor suppressor Merlin/NF2. Cell 154, 1342–1355 (2013). [PubMed: 24012335]
21. Chan EH et al. The Ste20-like kinase Mst2 activates the human large tumor suppressor kinase Lats1. Oncogene 24, 2076–2086 (2005). [PubMed: 15688006]
22. Pearce LR, Komander D & Alessi DR The nuts and bolts of AGC protein kinases. Nature reviews. Molecular cell biology 11, 9–22 (2010). [PubMed: 20027184]
23. Hara K et al. Amino acid sufficiency and mTOR regulate p70 S6 kinase and eIF-4E BP1 through a common effector mechanism. The Journal of biological chemistry 273, 14484–14494 (1998). [PubMed: 9603962]
24. Long X, Lin Y, Ortiz-Vega S, Yonezawa K & Avruch J Rheb binds and regulates the mTOR kinase. Current biology : CB 15, 702–713 (2005). [PubMed: 15854902]
25. Inoki K, Li Y, Xu T & Guan KL Rheb GTPase is a direct target of TSC2 GAP activity and regulates mTOR signaling. Genes & development 17, 1829–1834 (2003). [PubMed: 12869586]
26. Tee AR, Manning BD, Roux PP, Cantley LC & Blenis J Tuberous sclerosis complex gene products, Tuberin and Hamartin, control mTOR signaling by acting as a GTPase-activating protein complex toward Rheb. Current biology : CB 13, 1259–1268 (2003). [PubMed: 12906785]
27. Hara K et al. Raptor, a binding partner of target of rapamycin (TOR), mediates TOR action. Cell 110, 177–189 (2002). [PubMed: 12150926]
28. Kim DH et al. mTOR interacts with raptor to form a nutrient-sensitive complex that signals to the cell growth machinery. Cell 110, 163–175 (2002). [PubMed: 12150925]
29. Sancak Y et al. PRAS40 is an insulin-regulated inhibitor of the mTORC1 protein kinase. Molecular cell 25, 903–915 (2007). [PubMed: 17386266]
30. Sancak Y et al. The Rag GTPases bind raptor and mediate amino acid signaling to mTORC1. Science 320, 1496–1501 (2008). [PubMed: 18497260]
31. Peterson TR et al. DEPTOR is an mTOR inhibitor frequently overexpressed in multiple myeloma cells and required for their survival. Cell 137, 873–886 (2009). [PubMed: 19446321]
32. Thoreen CC et al. An ATP-competitive mammalian target of rapamycin inhibitor reveals rapamycin-resistant functions of mTORC1. The Journal of biological chemistry 284, 8023–8032 (2009). [PubMed: 19150980]
33. Laplante M & Sabatini DM Regulation of mTORC1 and its impact on gene expression at a glance. Journal of cell science 126, 1713–1719 (2013). [PubMed: 23641065]

34. Duvel K et al. Activation of a metabolic gene regulatory network downstream of mTOR complex 1. Molecular cell 39, 171–183 (2010). [PubMed: 20670887]

35. Dibble CC & Manning BD Signal integration by mTORC1 coordinates nutrient input with biosynthetic output. Nature cell biology 15, 555–564 (2013). [PubMed: 23728461]

36. Wei W et al. Degradation of the SCF component Skp2 in cell-cycle phase G1 by the anaphase-promoting complex. Nature 428, 194–198 (2004). [PubMed: 15014503]

37. Boehm JS, Hession MT, Bulmer SE & Hahn WC Transformation of human and murine fibroblasts without viral oncoproteins. Mol Cell Biol 25, 6464–6474 (2005). [PubMed: 16024784]

38. Yuan M, Breitkopf SB, Yang X & Asara JM A positive/negative ion-switching, targeted mass spectrometry-based metabolomics platform for bodily fluids, cells, and fresh and fixed tissue. Nature protocols 7, 872–881 (2012). [PubMed: 22498707]

39. Guo J et al. pVHL suppresses kinase activity of Akt in a proline-hydroxylation-dependent manner. Science 353, 929–932 (2016). [PubMed: 27563096]

40. Xie J et al. Short DNA Hairpins Compromise Recombinant Adeno-Associated Virus Genome Homogeneity. Mol Ther 25, 1363–1374 (2017). [PubMed: 28462820]

41. Grieger JC, Choi VW & Samulski RJ Production and characterization of adeno-associated viral vectors. Nature protocols 1, 1412–1428 (2006). [PubMed: 17406430]

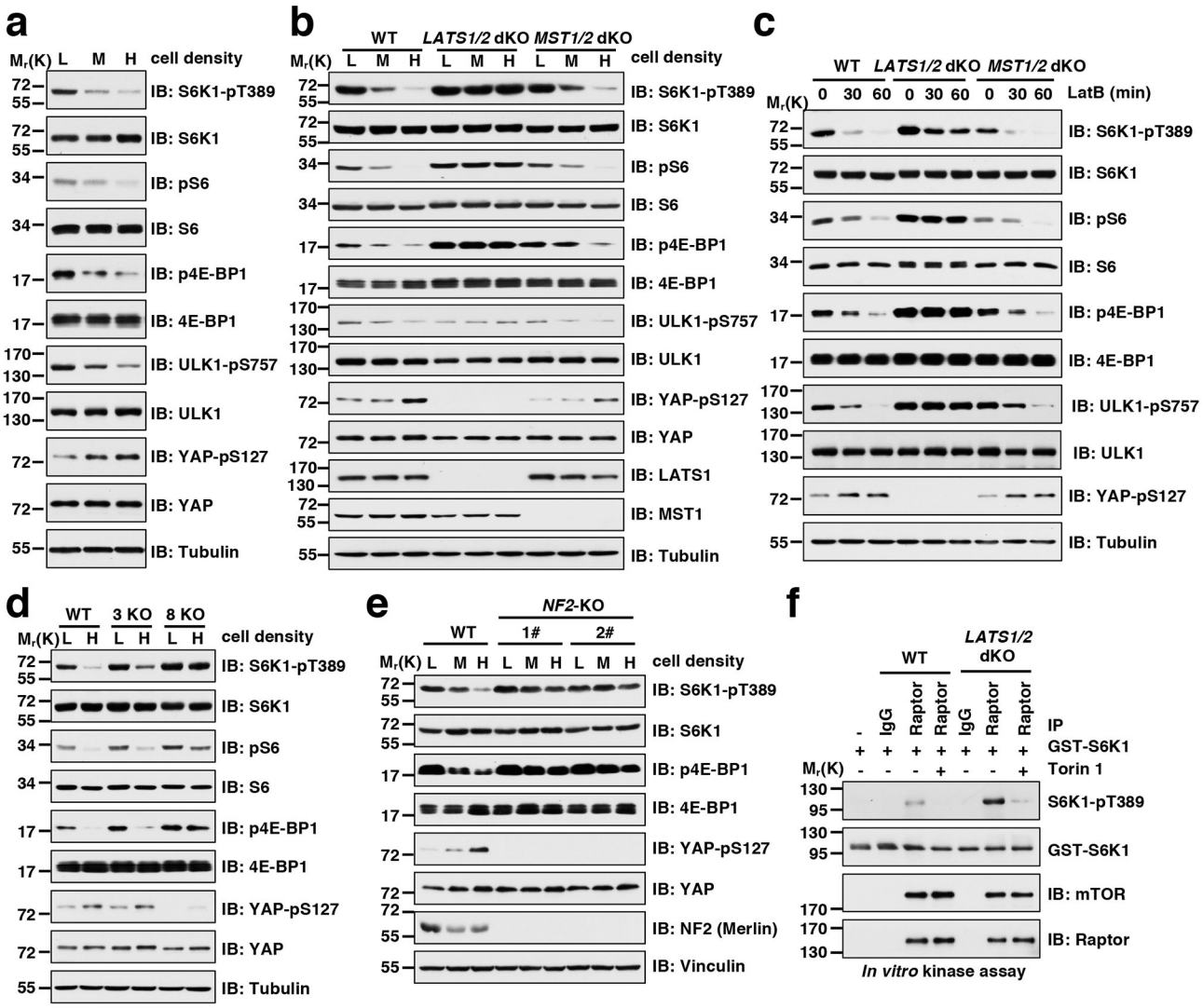


**Fig. 1. The Hippo pathway negatively regulates mTORC1 signaling via LATS1/2 kinases**

**a.** Increasing cell density attenuates mTORC1 kinase activity. HEK293 cells were seeded on 60 mm dishes at 30% (L), 60% (M) and 100% (H) confluence for 16 hours and then replaced with fresh medium for 1 hour before harvesting for immunoblot (IB) analysis.

**b.** *LATS1/2* dKO restores mTORC1 kinase activity at high cell density. 293A-WT, *LATS1/2* dKO and *MST1/2* dKO cells were cultured at 30% (L), 60% (M) and 100% (H) confluence for 16 hours and then replaced with fresh medium for 1 hour before harvesting for IB analysis.

**c.** mTORC1 kinase activity is reduced in 293A-WT and *MST1/2* dKO, but not *LATS1/2* dKO cells treated with 1 μg/ml Latrunculin B (LatB) for indicated time period.

**d.** IB analysis of whole cell lysates (WCL) derived from 293A-WT, *MAP4K4/6/7* (3KO) and *MAP4K1/2/3/4/6/7 MST1/2* (8KO) cells at 30% (L) and 100% (H) confluence.

**e.** IB analysis of WCL derived from 293-WT and *NF2*-KO cells at 30% (L), 60% (M) and 100% (H) confluence.

In vitro kinase assays demonstrate that genetic deletion of LATS1/2 leads to increased mTORC1 kinase activity *in vitro* towards phosphorylating S6K1. Raptor immunoprecipitates (IP) were prepared from 293A-WT or *LATS1/2* dKO cells and used for examination of mTORC1 kinase activity *in vitro*. Western blots in **a-f** were performed n=2 independent experiments, with similar results obtained. Unprocessed immunoblots are shown in Source Data Fig. 1.

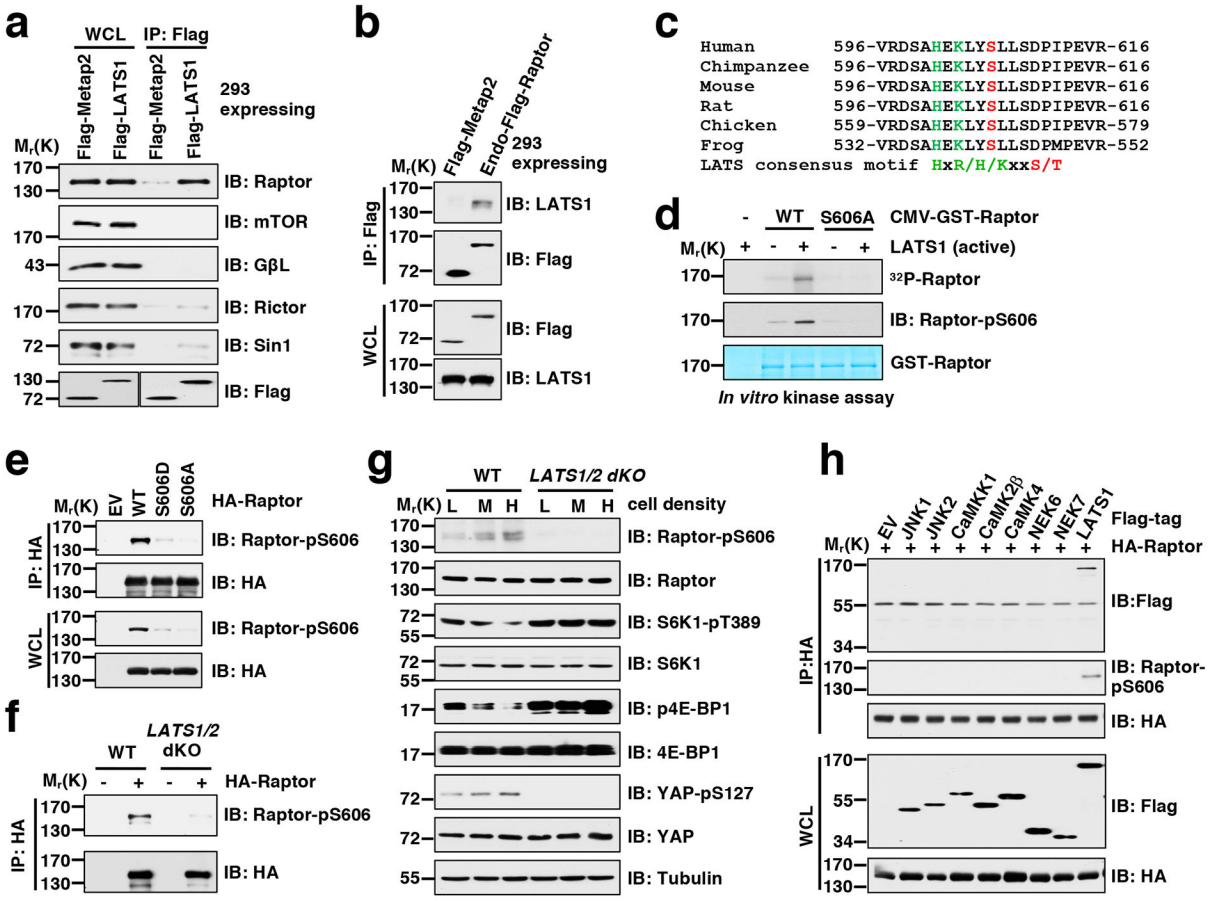


**Fig. 2. LATS1/2 kinases bind and phosphorylate Raptor**

**a.** LATS1 mainly interacts with Raptor in cells. IB analysis of whole cell lysates (WCL) and Flag-IP derived from stably expressing Flag-Metap2 or Flag-LATS1 HEK293 cells.

**b.** Endogeneous Raptor binds endogeneous LATS1 in cells. IB analysis of WCL and IP derived from 293 cells expressing Flag-Metap2 or endogenous-Flag-Raptor.

**c.** A schematic presentation of the evolutionarily conserved putative LATS1/2 phosphorylation site, Ser606, in Raptor.

**d.** *In vitro* kinase assays demonstrate that S606 is the major LATS1 phosphorylation site in Raptor. GST-Raptor fusion protein was purified from HEK293 cells and recombinant active LATS1 kinase was used as the source of kinase. Both Phosphorus-32 ($^{32}$P) isotope and anti-Raptor-pS606 antibody were used to detect phosphorylated Raptor species.

**e.** S606A or S606D mutation blocks Raptor-S606 phosphorylation recognized by the anti-Raptor-pS606 antibody. IB analysis of WCL and IP derived from 293 cells transfected with indicated constructs.

**f.** LATS1/2 are the major kinases for Raptor-pS606. IB analysis of WCL and IP derived from 293A or 293A-*LATS1/2* dKO cells transfected with indicated constructs.

**g.** *LATS1/2* dKO blocks Raptor-S606 phosphorylation. IB analysis of WCL derived from 293-WT, *LATS1/2* dKO cells at 30% (L), 60% (M) and 100% (H) confluence.

**h.** LATS1 specifically binds and phosphorylates Raptor. IB analysis of WCL and IP derived from 293 cells transfected with indicated constructs.

Western blots in **a, b, d-h** were performed n=2 independent experiments, with similar results obtained. Unprocessed immunoblots are shown in Source Data Fig. 2.

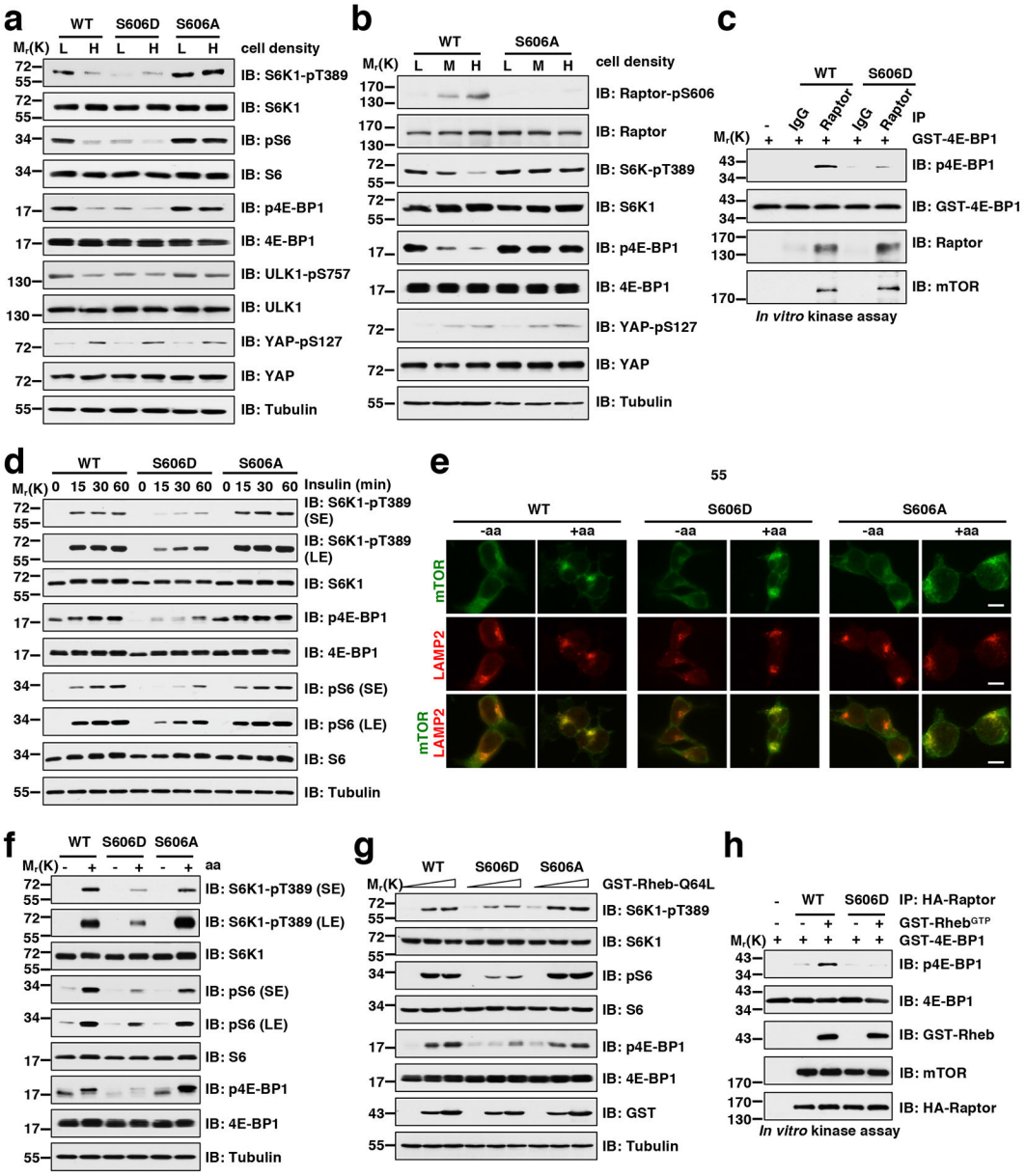


**Fig. 3. Raptor-S606D mutation inhibits growth factor-induced mTORC1 activation**

**a.** High cell density inhibits mTORC1 activity in parental, but not S606D$^{knock\text{-}in}$ or S606A$^{knock\text{-}in}$ HEK293 cells. IB analysis of WCL derived from WT, S606D$^{knock\text{-}in}$ or S606A$^{knock\text{-}in}$ HEK293 cells cultured at L (30%) or H (100%) confluence for 16 hours before harvesting.

**b.** Increasing cell density induces Raptor-pS606 signal in WT, but not S606A$^{knock\text{-}in}$ cells. IB analysis of WCL derived from HEK293-WT or S606A$^{knock\text{-}in}$ cells cultured at 30% (L), 60% (M) and 100% (H) confluence.

**c.** *In vitro* kinase assays demonstrate that phospho-mimetic mutation in S606 (S606D) leads to reduced mTORC1 kinase activity in vitro towards phosphorylating 4E-BP1. Raptor-IP derived from HEK293-WT or S606D$^{knock\text{-}in}$ cells were analyzed for mTORC1 kinase activity.

**d.** The Raptor S606D mutant is defective in timely activation of mTORC1 by insulin stimulation. The indicated CRISPR knock-in cells were serum-starved for 16 hours and then treated with 100 nM insulin for 15, 30 and 60 min before harvesting for IB analysis.
**e.** mTORC1 lysosomal localization is not affected in S606D$^{knock\text{-}in}$ cells. Cells were deprived of all amino acids (50 min) and stimulated with amino acids for 10 min prior to immunofluorescent co-labeling of mTOR with LAMP2. Scale bars, 10 μm. The experiment was performed n=2 independent experiments, with similar results obtained.
**f.** Amino acids fail to robustly activate mTORC1 in S606D$^{knock\text{-}in}$ cells. Cells were starved of all amino acids (50 min) and stimulated with amino acids for 10 min before harvesting.
**g.** The S606D mutation blocks Rheb-induced mTORC1 activation. IB analysis of WCL derived from indicated CRISPR knock-in cells transfected with constitutive active form of Rheb (GST-Rheb-Q64L). The cells were serum-starved for 16 hours before harvesting.
**h.** Rheb$^{GTP}$ fails to induce the activation of mTORC1 immunopurified from Raptor-S606D expressing cells *in vitro*. HA-Raptor-WT and S606D IP derived from HEK293 cells were analyzed for mTORC1 kinase activity toward 4E-BP1 in the presence or absence of Rheb$^{GTP}$.
Western blots in **a-d, f-h** were performed n=2 independent experiments, with similar results obtained. Unprocessed immunoblots are shown in Source Data Fig. 3.

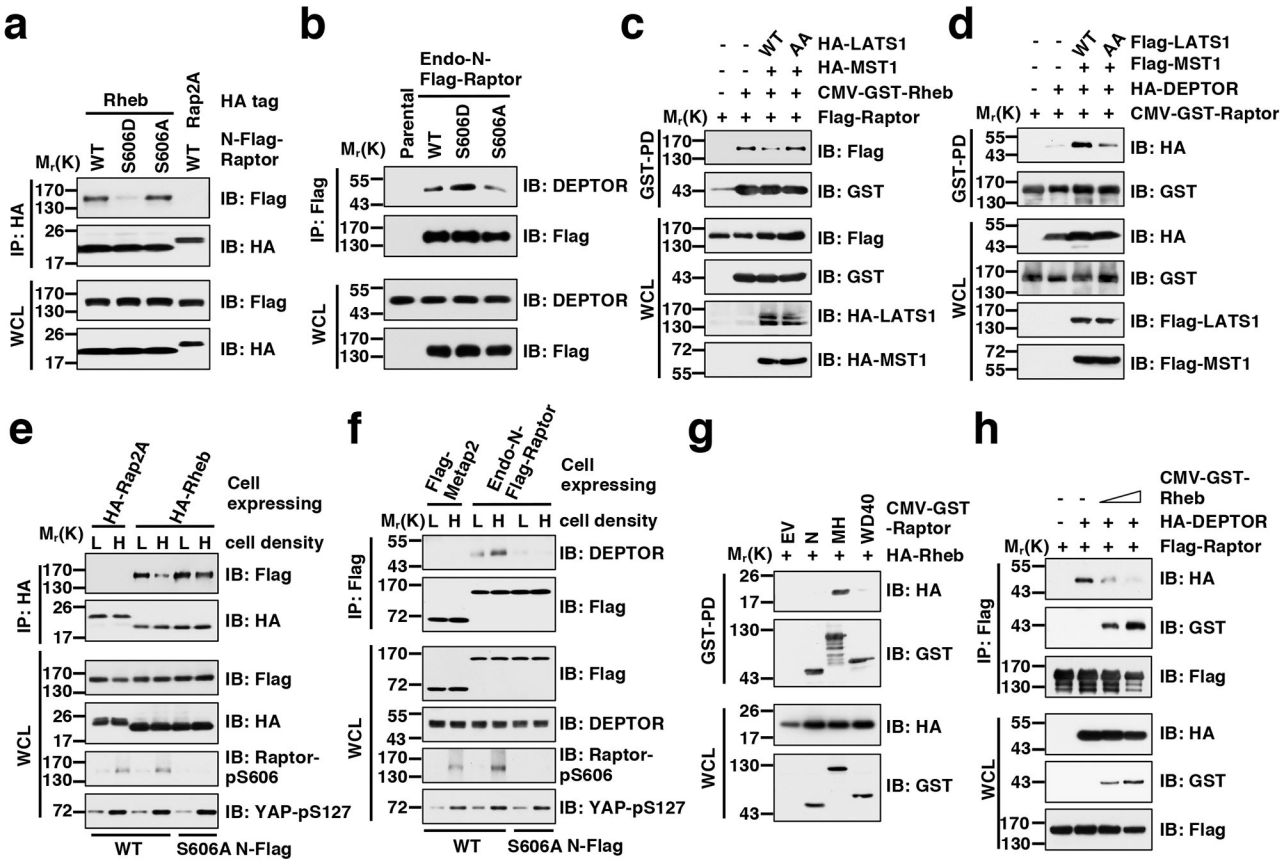


**Fig. 4. Raptor-S606 phosphorylation inversely regulates Raptor interaction with Rheb and DEPTOR**

**a.** The Raptor-S606D mutation impairs its binding with Rheb. IB analysis of WCL and IP derived from indicated CRISPR knock-in cells expressing HA-tag Rheb or Rap2A (as a negative control).

**b.** The Raptor-S606D mutant enhances endogenous Raptor and DEPTOR interaction. IB analysis of WCL and IP derived from indicated CRISPR knock-in cells.

**c.** LATS1 impairs Raptor interaction with Rheb in a kinase activity-dependent manner. IB analysis of WCL and IP derived from 293 cells transfected with indicated constructs.

**d.** LATS1 enhances Raptor interaction with DEPTOR. IB analysis of WCL and IP derived from 293 cells transfected with indicated constructs.

**e.** High cell density reduces Raptor-WT, but not Raptor-S606A, interaction with Rheb. IB analysis of WCL and IP derived from indicated cells expressed HA-tag Rheb or Rap2A (as a negative control).

**f.** High cell density enhances Raptor-WT, but not Raptor-S606A, interaction with endogenous DEPTOR. IB analysis of WCL and IP derived from indicated cells.

**g.** Rheb binds Raptor via the MH domain. IB analysis of WCL and IP derived from 293 cells transfected with indicated constructs.

**h.** Rheb disrupts Raptor and DEPTOR interaction in a dose-dependent manner. IB analysis of WCL and IP derived from HEK293 cells transfected with indicated constructs.

Western blots in **a-h** were performed n=2 independent experiments, with similar results obtained. Unprocessed immunoblots are shown in Source Data Fig. 4.

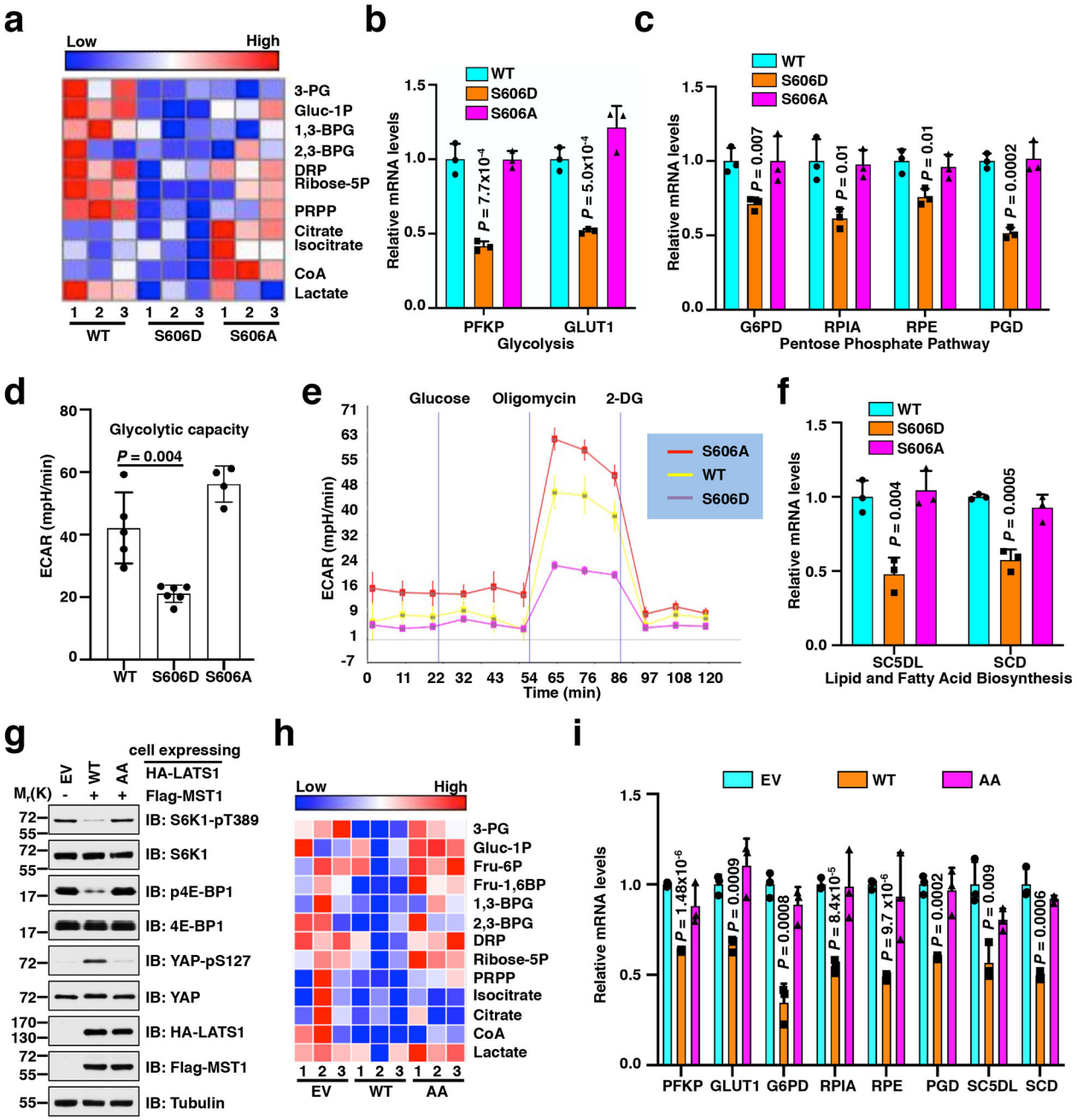


**Fig. 5. The Raptor S606D mutation suppresses glycolysis and lipid biosynthesis.**

**a.** Metabolomic profiling to show that compared to WT and S606A$^{knock\text{-}in}$ cells, S606D$^{knock\text{-}in}$ cells exhibit a decrease in metabolites of the glycolysis and pentose phosphate pathways. Relative levels of specific metabolites, normalized to cell number, from n=3 biologically independent samples for each cell line are shown in the heat map with dark blue and red representing the lowest and highest levels, respectively.

**b-c.** Real-time PCR assays to examine mRNA levels of representative genes in the glycolysis and pentose phosphate pathways. Data were shown as mean ± s.d. of n=3 independent experiments. *P* values were calculated using two-tailed Student's t-test.

**d-e.** ECAR analyses of glycolysis of 293-WT, S606D$^{knock\text{-}in}$ and S606A$^{knock\text{-}in}$ cells. Data were shown as mean ± s.d. n=5 biologically independent samples for WT, n=6 biologically independent samples for S606D, n=4 biologically independent samples for S606A. *P* values were calculated using two-tailed Student's t-test.

**f.** Real-time PCR assays to examine mRNA levels of representative genes of lipid and fatty acid biosynthesis. Data were shown as mean ± s.d. of n=3 independent experiments. *P* values were calculated using two-tailed Student's t-test.

**g.** LATS1-WT, but not kinase-dead mutant form of LATS1 (termed as AA) suppresses mTORC1 signaling. Immunoblot (IB) analysis of whole cell lysates (WCL) derived from LATS1-WT or AA expressing 293 cells. Blot is representative of n=2 independent experiments, with similar results obtained.

**h.** Metabolomic profiling to show that LATS1-WT, but not LATS1-AA expressing 293 cells exhibit a decrease in metabolites of the glycolysis and pentose phosphate pathways. Relative levels of specific metabolites, normalized to cell number, from n=3 independent samples for each cell line were shown in the heat map with dark blue and red representing the lowest and highest levels, respectively.

**i.** Real-time PCR assays to examine mRNA levels of representative genes of the glycolysis, pentose phosphate pathway and lipid and fatty acid biosynthesis. Data were shown as mean ± s.d. of n=3 independent experiments. *P* values were calculated using two-tailed Student's t-test.

Unprocessed immunoblots are shown in Source Data Fig. 5. Statistical source data are available in Statistical Source Data Fig 5.

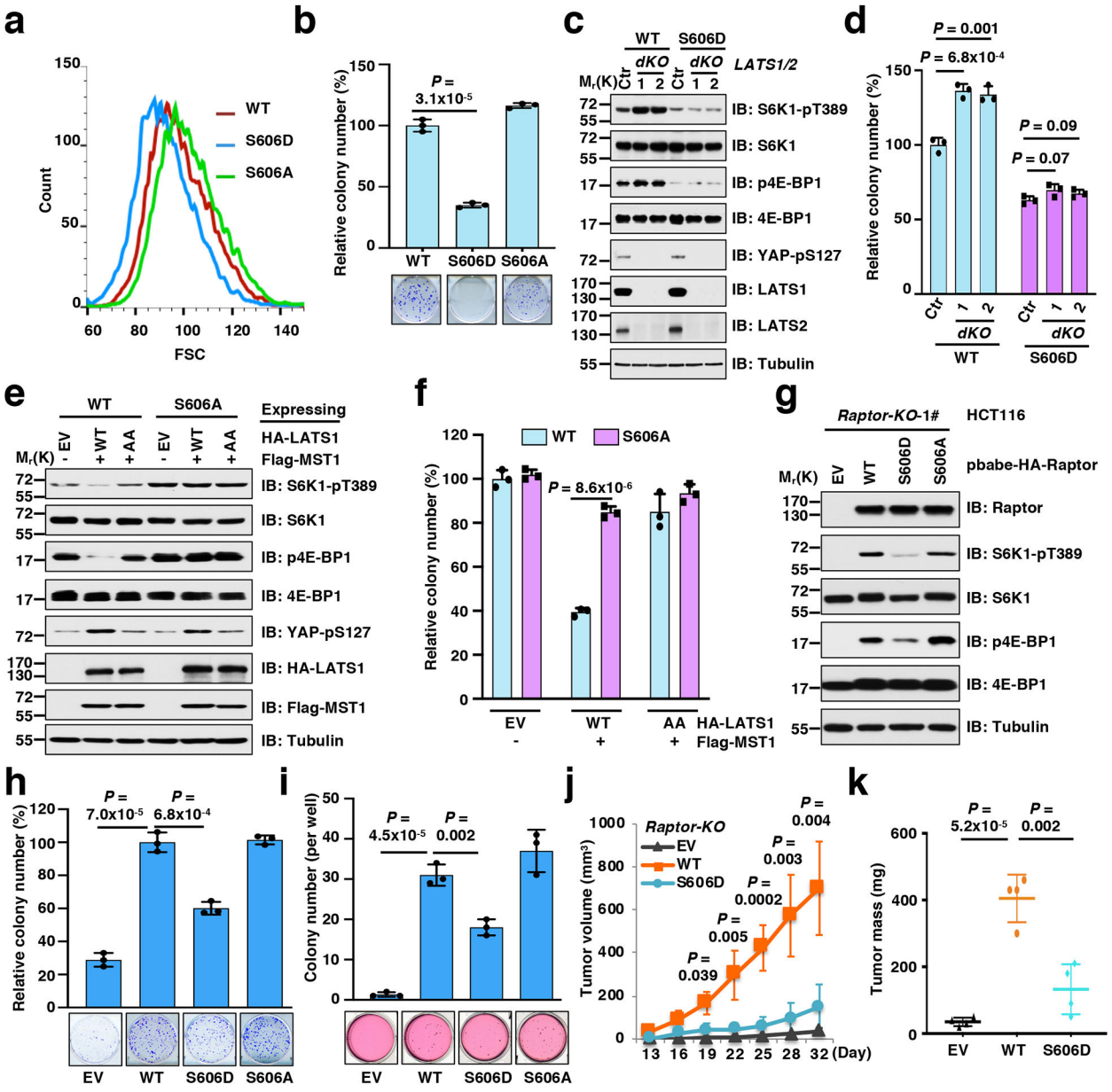


**Fig. 6. Raptor-S606D mutation suppresses cell growth and proliferation**

**a.** S606D*knock-in* HEK293 cells display smaller cell size than WT and S606A*knock-in* cells. Cells were grown in 10% serum at sub-confluence and subjected to cell size analysis by flow cytometry. The experiment was performed n=3 biologically independent experiments with similar results obtained.

**b.** S606D*knock-in* cells display reduced colony formation ability than WT and S606A*knock-in* cells. The CRISPR knock-in cell lines were plated for colony formation assays for 12 days. Data were shown as mean ± s.d. of n=3 independent experiments.

**c.** CRISPR-mediated *LATS1/2* knockout elevates mTORC1 activity in 293-WT, but not S606D*knock-in* cells. IB analysis of WCL derived from indicated cells. Blot is representative of n=2 independent experiments, with similar results obtained.

**d.** *LATS1/2* knockout increases colony formation ability of 293-WT but not S606D$^{knock\text{-}in}$ cells. Data were shown as mean ± s.d. of n=3 independent experiments.
**e.** Ectopic overexpression of LATS1 suppresses mTORC1 activity in 293-WT, but not S606A$^{knock\text{-}in}$ cells. IB analysis of WCL derived from indicated cells. Blot is representative of n=2 independent experiments, with similar results obtained.
**f.** Ectopic overexpression of LATS1 decreases colony formation ability of 293-WT, but not S606A$^{knock\text{-}in}$ cells. Data were shown as mean ± s.d. of n=3 independent experiments.
**g.** IB analysis of WCL derived from *Raptor*$^{KO}$ cells stably reintroducing Raptor-WT, S606D or S606A. Blot is representative of n=2 independent experiments, with similar results obtained.
**h-i.** Colony formation assays and soft agar assays demonstrate the deficiency of cell transforming ability for S606D expressing cells. Data were shown as mean ± s.d. of n=3 independent experiments.
**j.** *Raptor* knockout HCT116 cells stably reintroducing Raptor-WT or S606D (with EV as a negative control) were injected into nude mice. The tumor growth was monitored for indicated time period. Data were shown as mean ± s.e.m., n = 4 mice.
**k.** The weights of the tumors. Data were shown as mean ± s.e.m., n = 4 mice.
*P* values in **b, d, f, h-k** were calculated using two-tailed Student's t-test. Unprocessed immunoblots are shown in Source Data Fig. 6. Statistical source data are available in Statistical Source Data Fig 6.

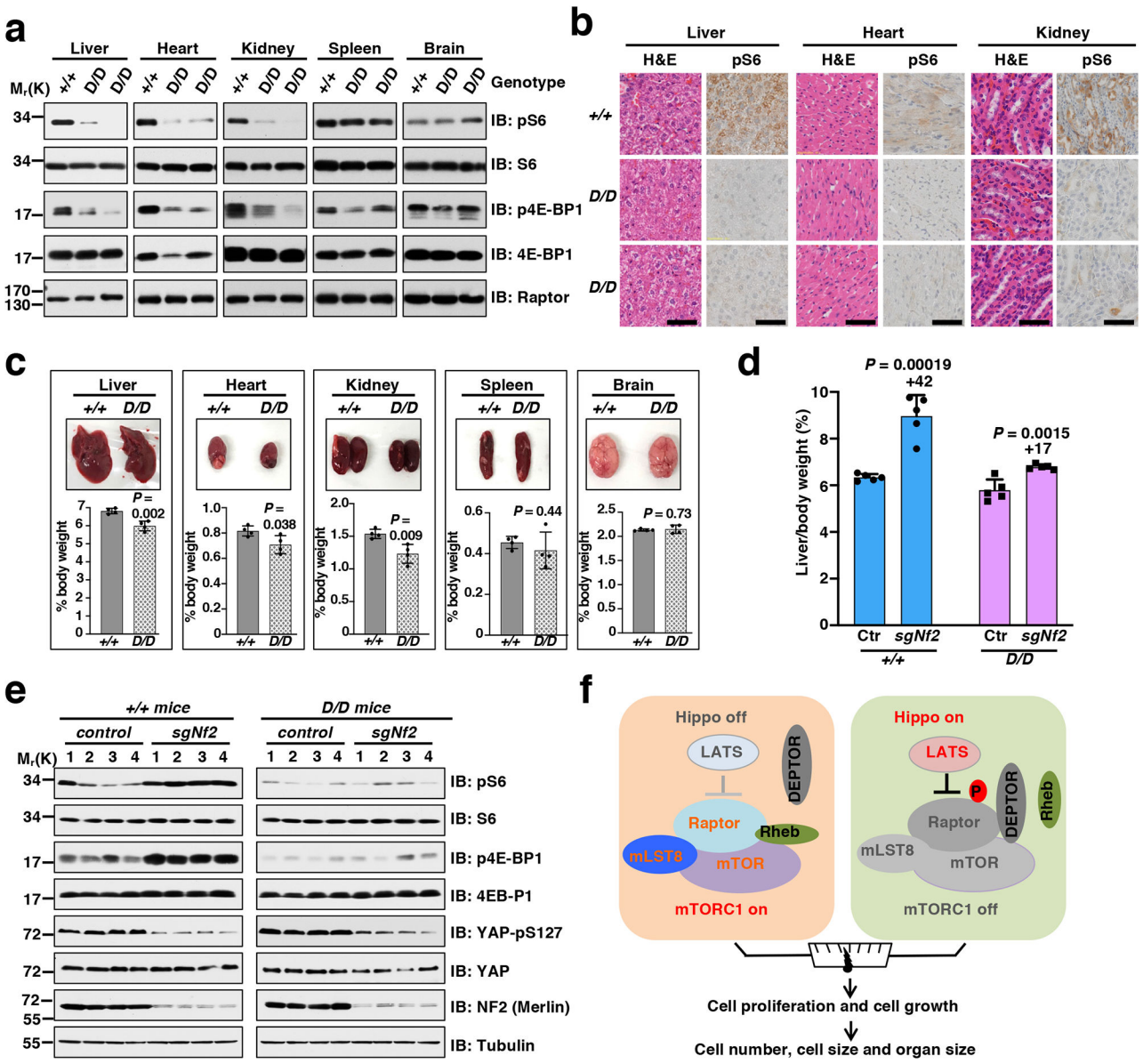


**Fig. 7. Phosphorylation of Raptor-S606 reduces mTORC1 activity and organ size in mouse**

**a.** IB analysis of WCL derived from indicated organs of 5-week-old *Raptor*$^{+/+}$ and *Raptor*$^{D/D}$ female mice. Blot is representative of n=2 independent experiments, with similar results obtained.

**b.** Organ sections prepared from 5-week-old *Raptor*$^{+/+}$ and *Raptor*$^{D/D}$ female mice were analyzed by immunohistochemistry for pS6 (pS235/S236) levels and stained with haematoxylin and eosin (H&E). Scale bars, 50 μm. n=2 independent experiments, with similar results obtained.

**c.** Representative images and organ weights of the 8-week-old female mice of *Raptor*$^{+/+}$ and *Raptor*$^{D/D}$. Data were shown as mean ± s.e.m. (n = 4 mice). *P* values were calculated using two-tailed Student's t-test.

**d.** *Raptor*$^{D/D}$ mice display relatively less increase of liver weight than *Raptor*$^{+/+}$ mice with AAV-mediated knockout of *Nf2*. Data were shown as mean ± s.e.m. Liver weight was shown as percentage of body weight (n = 5 mice). The percentage changes in liver weight compared to respective control mice are indicated. *P* values were calculated using two-tailed Student's t-test.

**e.** Adeno-associated virus (AAV)-mediated knockout of *Nf2* elevates mTORC1 signaling in *Raptor*$^{+/+}$ but not *Raptor*$^{D/D}$ mice. IB analysis of WCL derived from livers of *Raptor*$^{+/+}$ and *Raptor*$^{D/D}$ male mice depleted *Nf2* by the AAV-CRISPR system. Blot is representative of n=2 independent experiments, with similar results obtained.

**f.** A proposed model to describe the coordination between Hippo and mTORC1 pathways in synergistic regulation of cell proliferation, growth, organ size and body size.

Unprocessed immunoblots are shown in Source Data Fig. 7. Statistical source data are available in Statistical Source Data Fig 7.